Structural Characteristics of Aluminum-made Chassis-type Frame of a Tractor

Division of Agricultural and Forest Engineering
Doctoral Degree Program in Agricultural Sciences
University of Tsukuba

Muhaemin Mimin

Table of contents

Notation

δ	Deflection, m
δ_a	Maximum deflection in aluminum model, m
δ_s	Maximum deflection in steel model, m
ε_1	Strain in 1-direction
ε_2	Strain in 2-direction
ε_3	Strain in 3-direction
ε_{max}	Maximum strain
ε_{min}	Minimum strain
γ	Angle between the assumed centrifugal force and the tipping plane, radian
ϕ	Eigenvector
λ	Eigenvalue
μ	Poisson's ratio
σ	Stress, MPa
σ_1	Major principal stress, MPa
σ_2	Intermediate principal stress, MPa
σ_3	Minor principal stress, MPa
σ_s	Maximum stress for steel model, MPa
σ_y	Yield stress, MPa
υ_s	Critical speed, m/s
C	Horizontal distance between center of gravity and tipping line, m

E	Young's modulus, MPa
F_{cf}	Centrifugal force, N
g	Acceleration of gravity, m/s^2
I	Area moment inertia, m^4
I_x	Area moment of inertia with respect to x-axis, m^4
I_y	Area moment of inertia with respect to y-axis, m^4
J	Polar moment of inertia, m^4
$\{K\}$	System's stiffness matrix
L	Length, m
m	Mass, kg
$\{M\}$	System's mass matrix
P_μ	Scale factor of Poisson's ratio
P_δ	Scale factor of deflection
P_σ	Scale factor of stress
P_E	Scale factor of Young's modulus
P_F	Scale factor of force
P_L	Scale factor of length
P_M	Scale factor of moment
Q_1	Reading from individual gage 1
Q_2	Reading from individual gage 2
Q_3	Reading from individual gage 3
r	Tractor's turning radius, m
$\{R\}$	System's load vector

S	Strength ratio
T	Coefficient of strain gage's transverse sensitivity
{U}	Displacement vector
z_{cg}	Height of the center of gravity of a tractor, m

List of tables

List of figures

Only a few works have so far been done regarding mass reduction of agricultural tractor. One of the related works was conducted by Motobayashi *et al.*[41] in which the shape of side-member of a chassis-type frame was optimized and its mass was reduced by approximately 42%. Despite this pioneering achievement, the shape of the optimized model became somewhat complicated such that some manufacturing difficulties remained.

Another approach of mass reduction includes the adoption of lighter materials. Some strong but lighter materials, *i.e.* carbon fiber reinforced plastics, glass fiber reinforced plastics and aluminum alloys, are getting popular in various manufacturing aspects. Among these materials, aluminum is considered as one of the most reasonably priced candidate material. Moreover, it does not require drastic changes in production facility such that initial investment may be less[3]. Compared to other material, aluminum is more advantageous in terms of recyclability and, now, it is the second most recycled material after steel in the automotive industry*, [37].

Despite the fact that aluminum has been suggested as a material for future tractor by Taniguchi[56] as early as 1990, up to now there has been no published study dealing with this topic.

1.2 Objectives

The objective of this research was to reduce mass of a chassis-type

* Jost, K. 1995. Auto steel recycling approaches 100% annually. Automotive Engineering, 103(8): 43-45.

frame of a tractor by using aluminum without sacrificing its strength and stiffness. Two steps of research were conducted. For the first step, aluminum was used into an existing steel design, which have similar configuration. This was provided mainly to investigate the potential of aluminum for mass reduction of a steel structure. For the second step, to enhance the extent of mass reduction and improve the characteristics of aluminum frame, the shape of aluminum members was modified and its mass was minimized. Evaluation of strength and stiffness was conducted numerically using finite element method (FEM) as well as experiment. Finally, the effect of this structural modification to natural frequency was also investigated.

Chapter 2
Literature review

2.1 Types of tractor frame

There are two types of frame currently used by agricultural tractor: monocoque- and chassis-type frame (Fig. 2.1). Monocoque-type frame, a structure composed of engine block, transmission case, and rear axle housing connected rigidly with bolts, was first introduced by Henry Ford in 1917 with his famous Fordson model and up to now has been dominating the design of agricultural tractor. This frame allows the drive line elements to be perfectly encapsulated and well lubricated, and because it is made of cast iron it provides low first cost. However, since engine is directly connected to the tractor body, vibration from the engine is transmitted to whole body of tractor[50].

Another type of frame, the chassis-type frame, formerly used only with German garden tractor and special vehicles such as Unimog and MB-tracs. The usage of this type of frame in standard tractor started with the East German standard tractor ZT 300/303 and ZT 320/323. These tractors used half-frame to reinforce durability around the engine, simplify front attachments, and reduce noise by mounting the engine on elastic materials. Based on the study of these tractors, Matthies and Rohrs proposed the investigation of full-frame for standard tractor in 1984. Following this, in 1988 Kirste and Rhenius developed full-frame research tractor, and later,

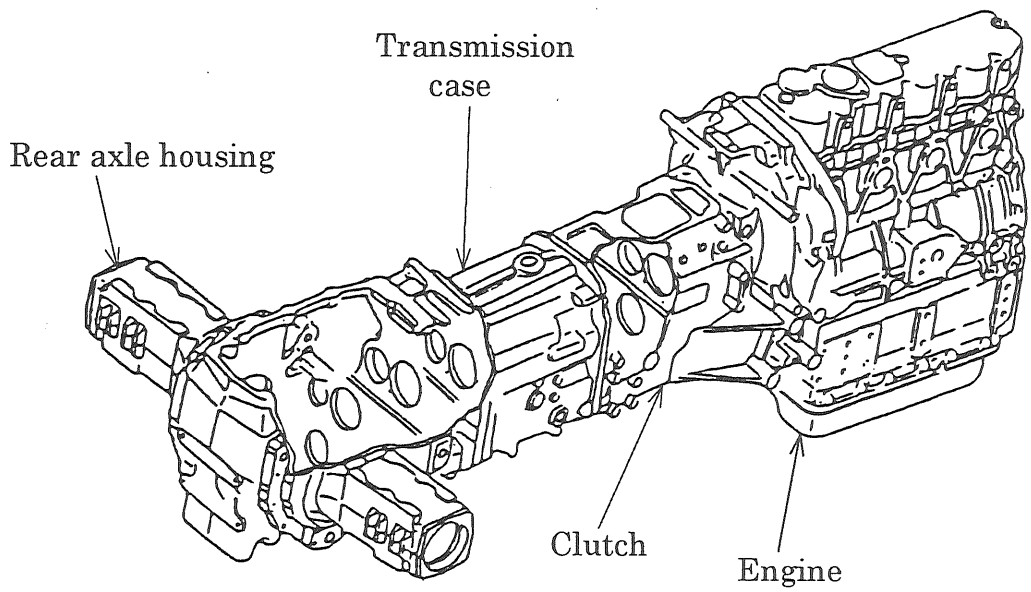

(a)

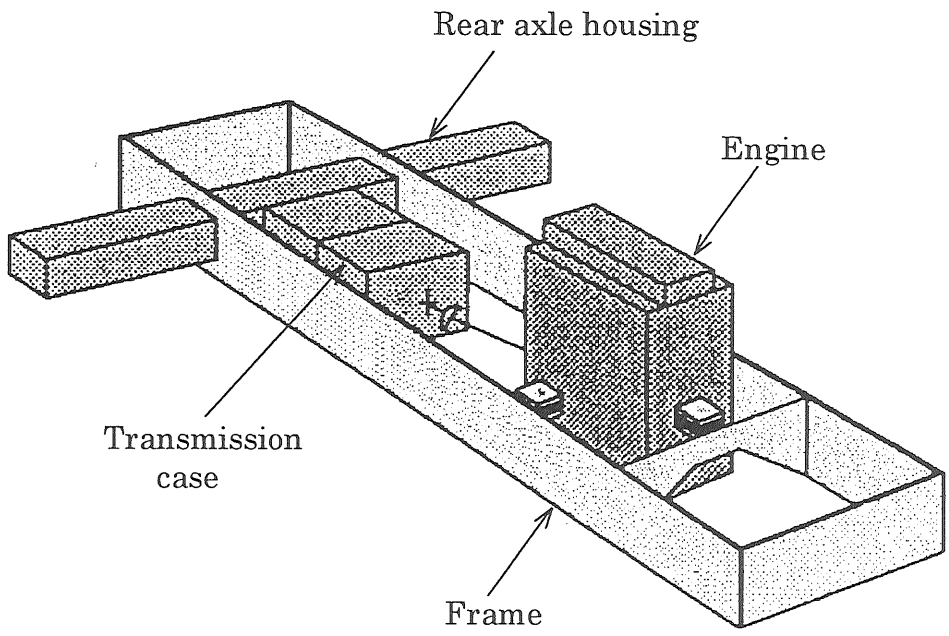

(b)

Fig. 2.1 Two types of tractor's frame: (a) monocoque- and (b) chassis-type.

tractor manufacturer begun to market its own version of full-frame tractor, such as Model 7000 and 6000 from John Deere in 1992[50]. As shown in Fig. 2(b), in tractor with this type of frame, engine, transmission case and rear axle housing are attached separately to the frame resulting in improved strength characteristics[56]. Furthermore, since strength is provided by the frame, other components can be made smaller and lighter. Full-frame research tractor presented by Kirste and Rhenius showed that tractor with this type of frame had lower mass compared to tractor with the monocoque one.[50] Other advantages are improved front hitch attachment, and better component flexibility. With the increasing popularity of front attached implements and demand on driving comfort, and emerging trends for tractor with lower specific mass, in the future it is likely that more tractors will adopt chassis-type frame instead of monocoque-type one.

2.2 Strength analysis of tractor structure

Due to tractor's pertinent role in agriculture, a great deal of researches on strength of its structure seems to be conducted more and more.

Garner[17] used stiffness matrix analysis to calculate the deflection and stress at any point in a monocoque-type frame. The frame was divided into a number of straight beams and flat panels. Results of the analysis were fairly confirmed by analytical solutions that treated the frame as a simple beam. Although the results from matrix analysis exhibited less accurate predictions at certain points, the study gave more information regarding the

diffusion of loads into the structure, the deflection of points in the structure, and the stress levels than what could be obtained by treating the tractor frame as a simple beam.

Koike and Tanaka[32] conducted basic analysis to clarify the structural damping of a tractor by theoretical and experimental means. In the theoretical analysis, the sinusoidal response characteristics of the tractor was clarified using a second order differential equation. It has been shown that the peak values in gain curves were due to manipulations of parameters, including the damping ratio and spring constant. The experimental analysis partly verified the possibility of parameter estimation by means of parameter manipulations. The experimental results also indicated the necessity for close attention to structural damping when dealing with the resilient vibration of a tractor frame.

In order to investigate the fatigue strength of the rear wheel axis housing, Koike and Tanaka[33] attached rosette strain gages on the rear wheel axis housing. Strain data were recorded for a tractor operating under the condition of tractor alone, with rotary, and with plow. The frequency of actual stress level from field tests tended to follow the Weibull distribution. Based on these results the service life of rear axle housing was predicted using Miner's damage law.

Nishizaki and Inooku[43] tested a 70 kW tractor by attaching strain gages on its front and rear axle housing to measure strain. Moreover, accelerometers were placed in front of an operator seat to measure

acceleration, and a torque transducer was housed to the PTO to measure transmitted torque during experiments on gravel road, concrete road, and field. As predicted, the PTO load on gravel road at tractor speed of 5.0 km/h was higher than that on concrete road even at PTO speed equal to five times of the tractor's speed. Furthermore, the load on front axle was always higher than that of rear axle. However, for running with rotary, the frequency at any speed was lower, in the range of 2.6–4.7 m/s^2. All frequency data were analyzed to produce power spectral density (PSD). Based on frequency analysis, it was obvious that major components of frequency at front and rear axle were below 5 Hz. The PSD distribution reached its peak values when the tractor run on gravel road.

Based on these test results, then actual load simulation of 3920 N with frequency of 5 Hz and maximum acceleration of 20 m/s^2 was performed[29]. The collected data were then used to predict the service life of related tractor components. According to the S-N curve, it was predictable that the remaining life of the frame was about 50 hours. In addition to load simulation, finite element study on modal analysis and on an experimental chassis-type frame was also carried out. Results showed that at frequency of 111.3 Hz, a huge deflection was detected at the center of the frame.

Using a 35-kW tractor installed with strain-gage-based load cell placed at the front and rear axle, Rahama and Chancellor[48] conducted two sets of experiments at a specially-designed paved roadway with wooden bumps and in a field representation typical to agricultural environment in order to

investigate forces which would contribute to the fatigue failure of different tractor components. Five different agricultural operations were used for field experiments, namely (a) plowing, (b) disk harrowing, (c) transporting with a front end loader, (d) carrying a heavy implement suspended on the three-point hitch, and (e) trailing a loaded wagon. Results from the experiment on paved roadway showed that the levels of speed used caused more variation in PSD magnitudes than the one of bump height used. In general, the dual bumps test produced data with essentially the same magnitudes and characteristics as was the case from the single bump test. For field operations, the interactions of the tractor and implement with the soil tended to minimize vibrational moment variations in high-frequency range. The differences in load imposed by disk harrowing, plowing, and cross-harrowing were reflected in PSD magnitudes only in the low-frequency range, *i.e.*, 0.5 to 4 Hz. It was also found that the mean stress, RMS cyclic stress values, and PSD values in the low-frequency range for field and transport operations were at the same approximate magnitudes as the stress values obtained with the 44 mm bumps encountered at a speed of 3.2 km/h. The data collected in this study were used to carry out fatigue life analysis of tractor axles.

To investigate the influence of design variables on the behavior of stress and deformation of monocoque-type frame at elastic-plastic zone, Hasegawa *et al.*[25] created three numerical simulation models of the frame, namely A-, B-, and C-model. The A-model was proposed taking selected specifications

from an existing 17.6 kW tractor and had a frame thickness of 10 mm. The B-model was basically the same as A-model except that its rear axle housing part was made thicker by 5 mm. On the other hand, the C-model was made by attaching one piece of partition wall into the rear axle housing part of the B-model. As predicted, analysis results showed that the stress and deformation were concentrated in the rear axle housing, and it was only in this part that plastic deformation was observed. Furthermore, under the same loading, the C-model exhibited higher values of stress and deflection, while A-model exhibited the lowest values.

2.3 Mass reduction and light weight materials

The size and mass of agricultural tractor has been steadily increased in the past. However, this trend seems to be leveling off. Survey on tractors from top ten companies in the Western Europe market showed that its specific mass decreased by 8% between 1982 and 1990. This was mainly achieved by increasing engine efficiency mostly with turbo-charging. Although, it was predicted that it is technically possible to further reduce the specific mass by 10% in the period of 1990 to 2000[50], up to now there are only a few published reports on research to reduce tractor mass.

Historically, the desire to reduce structural mass without compromising structural integrity, particularly in aircraft design, has been a strong driving force behind the development of structural optimization methods[4]. Today, some of the most successful applications of the method are in transportation

sector. While combustion engine is considered efficient enough[3], many efforts to reduce energy consumption and gas emission are directed to mass reduction of the vehicle[21,50]. Structural optimization has been also applied to reduce the mass of tractor frame[41].

The effectiveness of structural optimization as a tool to minimize mass of a structure is eventually limited by the property of used material. If further mass reduction is required, lightweight material could be adopted to replace a conventional one. In addition to having less density, some lightweight materials often have superior properties with respect to corrosion, machinability, and formability[27].

Some of the commonly used materials for lightweight vehicles are high-strength steel, aluminum, glass fiber reinforced plastics (GFRP) and carbon fiber reinforced plastics (CFRP). Before substituting lightweight materials for conventional ones, prediction on how much mass is likely to be saved by substitution must be conducted. The mass saving cannot be determined solely by comparing the density of the lightweight material to that of the conventional ones it replaces. A part's function and the engineering qualities of the material must also be taken into account, and when they are, the saving in mass is often to be much less than it would appear to be on the basis of density alone. For example, although the density of cast aluminum is 63% less than that of cast iron, the actual saving is much less, since greater volume of aluminum must be used to compensate for superior properties of the cast iron. If design constraint on the components is only equal stiffness

for both components, the mass saving derived from the substitution is only 11%[12].

Table 2.1 shows the property of several lightweight materials together with mild steel. Based on strength and stiffness alone, fiber reinforced composite materials, *i.e.* CFRP and GFRP, do not have clear advantage particularly if it is noted that their elongation to fracture is much lower than metals with comparable strength. However, since the materials are supposed to replace the conventional ones, more meaningful comparison is provided if density is also included. These are given by specific elastic modulus and specific tensile strength. In terms of elastic modulus, only CFRP is better than mild steel. For tensile strength, other materials except short, random-oriented GFRP are better than mild steel. By referring to mild and high-strength steel it can be asserted that for stiffness based design, high-strength steel offer no mass saving to mild steel, but it could derived considerable mass saving for strength-based design. For example, in the case of side door beams of a car that protect occupants from side impacts, high-strength steel could offer a mass saving of 18%[12]. Nevertheless, based on either stiffness or strength, CFRP offers the highest mass saving if it substitutes mild steel. Short, random-oriented GFRP can be used only in component that does not require high strength and stiffness such as interior of a car, cover of electrical instruments etc. In this case, mass saving may be predicted directly from material density.

Table 2.1 Property of material commonly used for mass saving

Material	Density, $Mg \cdot m^{-3}$	Elastic modulus, $GN \cdot m^{-2}$	Tensile strength, $MN \cdot m^{-2}$	Elongation to fracture, %	Specific modulus*	Specific tensile strength†
Mild steel[3]	7.8	207	172	18-25	26.5	22.0
High-strength steel[27]	7.8	207	up to 500	12-28	26.5	up to 64.1
Al-Zn-Mg alloy[27]	2.8	72	503	11	25.6	179.6
CFRP, epoxy resin, uni-directional laminae[27] (V_f‡=0.6)						
i) parallel to fiber	1.62	220	1400	0.8	135	865
ii) perpendicular to fiber	1.62	7	38	0.6		
GFRP, polyester resin unidirectional laminae[27] (V_f=0.5)						
i) parallel to fiber	1.93	38	750	1.8	19.7	390
ii) perpendicular to fiber	1.93	10	22	0.2		
GFRP, short, random-oriented fiber, polyester resin[27] (V_f=0.2)	1.55	8.5	110	2	5.5	71

* elastic modulus/density, $kN \cdot m \cdot g^{-1}$

† tensile strength/density, $kN \cdot m \cdot g^{-1}$

‡ volume fraction

Although specific elastic modulus and specific tensile strength is useful to roughly predict mass saving, a more precise prediction depends on the geometry of the component and the nature of the working load. For example, to minimize mass of a cantilever beam having square section under a single force at its end, at a certain value of deflection, the proper comparative index would be $E^{0.5}/\rho$ instead of specific elastic modulus, E/ρ[3].

CFRP and GFRP are different from isotropic material such as steel, that is, their property depends on direction. As can be seen in Table 2.1, for unidirectional laminae, strength and stiffness reach their maximum value at direction parallel to fiber and reach their minimum value at direction perpendicular to fiber. This very large difference in properties in different direction may be a serious limitation in some applications, but it may also become one of the outstanding advantages in other applications since it allows possibility of introducing stiffness and strength into a product where it is really required. In other words, it introduces an element of flexibility into design, but design is correspondingly more difficult and demanding[27].

The process of deciding which material to adopt does not stop when the mass saving has been computed. Cost is one of determining factors in decision making process. The price of several lightweight materials is given in Table 2.2. Because from one material there are many end-products in the market with different prices, the price of their respective raw materials was taken as base of comparisons. As can be seen in the table, lightweight materials are more expensive than the conventional ones. Aluminum is

Table 2.2 Price of steel and several lightweight materials

Material	Average price, $/t	Relative price
Steel ingot for casting	785[8)]	1.0
Aluminum ingot	1 313[64)]	1.7
Glass fiber*		
A-glass	1 709	2.2
C-glass	1 929	2.5
E-glass	1 929	2.5
S-glass	15 432	19.7
Carbon fiber*		
Heavy	23 149	29.5
Medium	38 581	49.1
Low	121 254	154.5
Aramid*		
Kevlar 29	28 660	36.5
Kevlar 149	60 627	77.2

about 70% more expensive than steel, while fiber glasses are about 2 - 20 time more expensive. Stronger fiber such as carbon and aramid are 30-150 times more expensive than the conventional materials. Currently, only certain high-strength steel is cost-effective on the basis of material cost alone. However, when fabrication cost, component integration advantages, facility and tooling cost are taken into account, aluminum and GFRP with A-, C-, and E-glass fiber are also seen to be cost-effective for certain applications. Plastics and, to a certain degree, aluminum offer advantages in the integration of components; since the material is easier to form, large assemblies, which originally would require many separate parts, can be molded as a single unit. On the other hand, because of very high cost, the

* Owens Corning Ltd. 1998. Fiber price list. New York, 1998.

application of carbon and aramid fiber can be justified only if mass or safety is the overriding design criterion such as in aircraft. Typical application for lightweight materials is presented in Table 2.3.

Table 2.3 Some applications of selected lightweight materials

Materials	Application
CFRP	Driveshaft for light trucks[30], flywheel rotor*
GFRP	Spring for heavy duty truck and trailer[30]
	Space frame of a prototype minivan†
	Multifunctional cross-member‡
	Seat lumber adjuster§
	Chain cover‖
	Body sheets[3]
	Clutch and accelerator pedal¶
Aluminum	Automobile space frame[6, 46, 47]
	Transmission housing[6, 46]
	Cylinder heads, intake manifold[6]
	Chassis frame of sports car#
	Drive shaft[7]

2.4 Environmental aspects of mass reduction

2.4.1 Reduction of energy consumption

With the increasing importance attached to the quality of life and concern over rising pollution levels, vehicle energy efficiency have become

* Jost, K. 1995. Composite flywheel rotors for hybrid EVs. Automotive Engineering, 103(10): 25-26.

† Anonymous. 1995. Material innovations: Composite body. Automotive Engineering, 103(1): 50.

‡ Anonymous.1995. Material innovation: Cross-vehicle beam. Automotive Engineering, 103(1): 53, 95.

§ Anonymous. 1995. Seat lumbar adjuster. Automotive Engineering, 103(2): 275.

‖ Anonymous. 1995. Timing chain cover. Automotive Engineering, 103(2): 275.

¶ Holt, D. 1995. Nylon pedal module. Automotive Engineering, 103(9): 18-19.

\# Birch, S. 1995. Renault's composite spider. Automotive Engineering, 103(7): 53-54.

focus of debate and legislation in the last two decades. In the past, energy analysis for alternative vehicle used to be conducted on partial basis, *e.g.*, energy analysis was mainly based on fabrication stage. Recently, the trend is to analyze energy on all stages, from material processing before vehicle fabrication to material disposal at the end of the vehicle's life.

Studies have been done to quantify the life-cycle energy consumption for conventional steel-made parts and aluminum ones of a vehicle. Figure 2.2 shows the life-cycle energy consumption of two parts of a car: hood and bumper reinforcement. In both parts, the energy for fabrication is less for steel than aluminum. However, the lifetime use of energy is much less for aluminum-made parts. Less fabrication energy is also observed in hood made of recycled aluminum. This lower life-cycle energy consumption is due to lower mass of aluminum parts. A reduction of mass by 10% could result in a gain of fuel economy by 4–7%[44]. The lighter the mass, the lesser energy is needed to move the vehicle during its lifetime, and the largest portion of total energy use is to operate the vehicle, not to build it.

Up to now there were little published study on lifetime energy consumption of agricultural tractor. Although there are differences between tractor and car in terms of assigned tasks, still some similarities in transport mechanism exist between them. Based on this consideration, these data from a car may serve as a preliminary and rough estimate on that of a tractor.

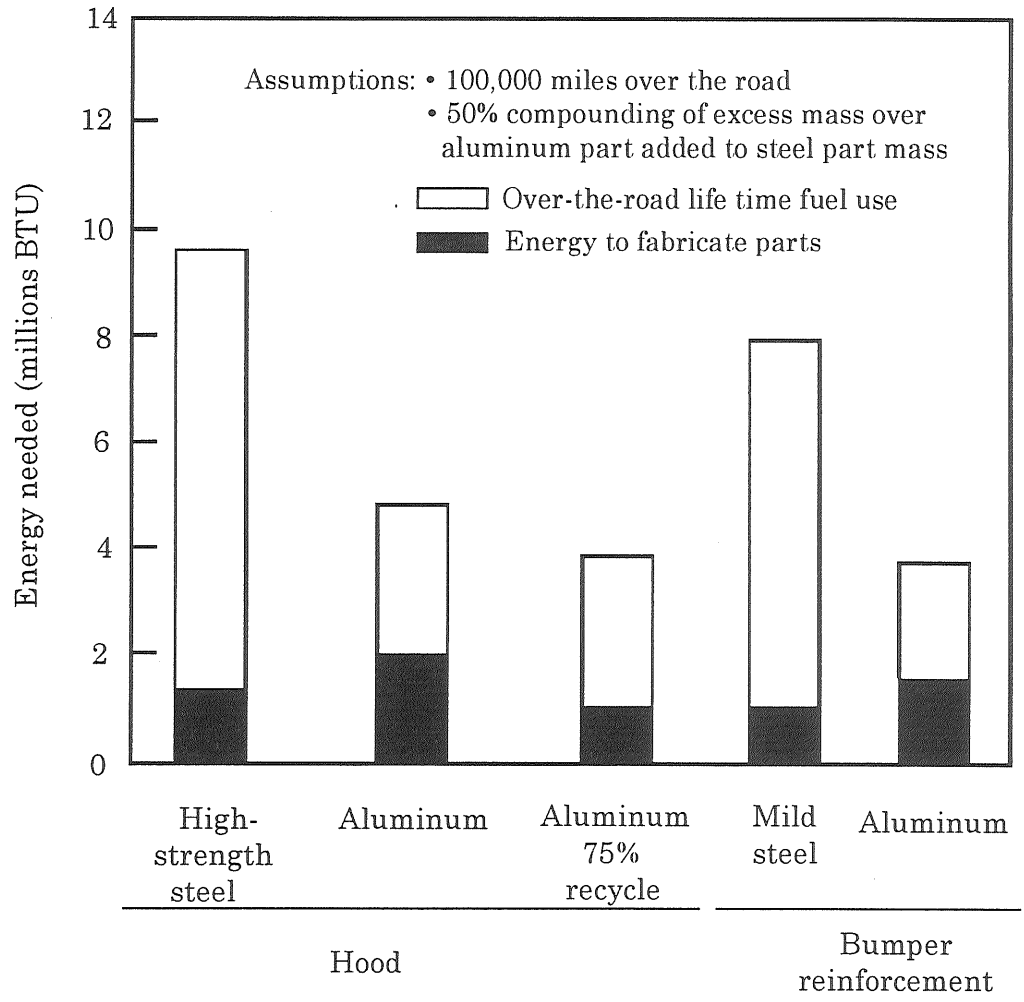

Fig. 2.2 Life-cycle energy consumption of steel and aluminum part of a car[44].

2.4.2 Reduction of soil degradation

It is well known that farm machinery, especially tractor, play an important part in soil compaction. In central Europe, during the last 3–4 decades, both the mass of agricultural machinery and the number of wheeling events have increased by over 300%. As a result, degraded soils due to compaction cover an area of about 33 Mha which approximately 50% of the physically degraded area of the world[45].

Soil compaction can broadly be divided into topsoil compaction and sub-soil compaction. Tillage and annual change in soil temperature and moisture due to natural causes can alleviate topsoil compaction within a few years. Nevertheless, sub-soil compaction at depths of over 40 cm can persist for decades[23]. At this depth, it is often difficult to alleviate compaction using mechanical means. Several investigations indicate that subsoil loosening can usually partly alleviate, and under inappropriate conditions, it may even cause soil deterioration[34].

Results from experiments in the former USSR showed that although compaction was usually concentrated in the upper 25–30 cm, several passes by 3–8 Mg tractors on moist soils caused compaction to a depth of 60 cm. Still, heavier agricultural, forestry or military vehicles were observed to cause compaction to depths of 0.8–1.0 m[23].

To avoid the risk of permanent compaction effects in the subsoil, stresses exerted by vehicles in the subsoil should not be allowed to exceed the internal soil strength. This can be achieved by limitation of axle load, or vehicle mass. For presently available large size tractors in the market, this means reduction of tractor's mass.

Chapter 3

First design modification of a tractor frame using aluminum

3.1 Introduction

The aluminum was selected as a material of construction for tractor frame because of its lower density compared to steel. Nevertheless, aluminum also has a lower strength and stiffness. On the other hand, design highly determines the characteristics of a structure. Before proceeding to design a new lightweight aluminum structure, it is necessary to understand the interaction between those factors in mass reduction effort with aluminum. Bearing this in mind, in this first approach aluminum will be used in existing steel frame design. This approach permits impartial comparison between the steel and aluminum structure.

A tractor is composed of various components with complex geometry. Before the development of numerical techniques, the complexity of the components made analytical prediction of structural behavior very difficult or even impossible such that test result and field data evaluation were the main tools for design improvement. Since high-speed digital computer became available, finite element method (FEM) has taken most parts of the design process[17, 42]. With the application of FEM, it is possible for design and analysis to be carried out in the same phase, which result in less testing time, fewer sample, and more reliable product.

FEM deals with known theory on a structure rather than the actual

structure itself. Because of this, the validity of its results may still questionable. In this respects model testing is necessary to find the relationship between the results of FEM and actual measurement on the model. In this study, numerical analysis as well as experiment was conducted on models with a scale factor of 1:2 instead of prototypes.

The specific objectives in this chapter were

1) To develop aluminum frame model with similar design and strength but at considerably lower mass compared to the existing steel model. The strength evaluation was conducted through numerical analysis with FEM.
2) To verify the validity of FEM program used in this study by comparing its results to that of loading tests.

3.2 Methodology

3.2.1 Similitude analysis

For an elastic structure having length L, force F and moment M, any component of stress σ and deflection δ at any specified point can be determined by the following equations[35];

$$\sigma = \frac{F}{L^2} f_1\left(\frac{F}{EL^2}, \frac{M}{FL}, \mu\right) \tag{3.1}$$

$$\delta = \frac{F}{EL} f_2\left(\frac{F}{EL}, \frac{M}{FL}, \mu\right) \tag{3.2}$$

where E is Young's modulus and μ is Poisson's ratio. These equations yield

the following general law of model for statically elastic structures,

$$P_\mu = 1, \quad P_F = P_E P_L^2, \quad P_M = P_F P_L, \quad P_\sigma = P_F / P_L^2, \quad P_\delta = P_L \tag{3.3}$$

where P_μ, P_F, P_L, P_M, P_σ, P_δ are scale factors of Poisson's ratio, force, length, moment, stress and deflection, respectively.

Based on equation (3.3), with the same value of Young's modulus and Poisson's ratio, and length scale factor P_L of 2, the ratio of force, stress and deflection between models and their prototypes have been determined to be 1:4, 1:1 and 1:2, respectively.

3.2.2 Numerical analysis

(a) Computing Facilities

In general, FEM analysis starts with pre-processing in which the geometry of the model, boundary conditions, and loading cases are defined. One outcome of this is an input file for a solver that serves to compute the solution. Then, a post-processing program in graphical or numerical mode displays the results from FEM. In this study, the pre- and post-processing software FEMAS (Finite Element Method Assist System) was used. This program was developed by Toyo Information System Co. Ltd., Tokyo, and intended to assist user in using widely available finite element solver programs by providing graphical modeling module for pre-processing

(FEMIS module)* and graphical display for post-processing (FEMOS module)†. FEMIS was furnished with a good user interface such that building finite element model became a less daunting task. On the other hand, graphical display for post-processing has only a few options and facilities for displaying output such that it might be difficult to represent output in the most desired way. File management system in both of the modules, FEMIS and FEMOS, was very poor. For example, user was not free to select the input file for processing and to name the output file, either text or graphics. In many cases, files were named by numbers such that more difficult to recognized later. This program could serves several popular finite element programs such as NASTRAN, ABAQUS, MARC, SAP, ELF and FEM5. FEMIS Translator served to translate the graphical finite element model, FEMIS save file, into input data for these programs‡.

Together with FEMAS, POPLAS/FEM5 (Problem Oriented Professional Library for Engineering Analysis and Simulation/Finite Element Method 5) developed by Fujitsu Co. Ltd., Tokyo, was employed as solver. This program consisted of modules for linear static analysis, eigenvalue analysis, modal analysis, and response spectrum analysis. Although in complete form it also includes module on structural optimization and heat transfer§, these

---

* Toyo Information System Co. Ltd. 1994. Finite Element Assist System FEMAS Ver. 8.1: FEMIS Subsystem User Manual, Vol. 1, Tokyo (In Japanese).
† Toyo Information System Co. Ltd.. 1994. Finite Element Assist System FEMAS Ver. 8.1: FEMOS Subsystem User Manual, Vol. 2, Tokyo (In Japanese).
‡ Toyo Information System Co. Ltd. 1994. Finite Element Assist System FEMAS Ver. 8.1: Interface Subsystem User Manual, Vol. 3, Tokyo (In Japanese).
§ Fujitsu Co. Ltd. 1995. POPLAS®/FEM5 Manual for V25 (Structural Analysis Program

modules were not installed in the computer at the Center for Science and Information Processing, University of Tsukuba. Beside the capability for solving FEM problems, the program also has various commands for creating FEM model. Nevertheless, the capability for creating model was severely limited because of having no graphical interface. It can be used for relatively simple FEM model only.

The process of numerical analysis with FEM using these two programs is given in Fig. 3.1. First, FEM model is created graphically using FEMIS module of FEMAS. Then FEMIS Translator converted the save file of FEMIS, *.gm_save, into input file for FEM5, *.gt_inp. This file is then fed to FEM5 program. For each input file there are three output files created by FEM5: save file, standard output, and log file. The numerical results can be read directly from standard output files. However, for better understanding graphical output is necessary. In this case, FEMOS Translator converts the FEM5 safe file, *.pt_outp, into three input files for FEMOS: *.pm_da07, *.pm_da17, and *.pm_da18. Then, using these files, FEMOS can display the FEM results graphically. FEMOS also has the capability to generate tabulated numerical results in various formats, which are easier to interpret than that of standard output file from FEM5.

The FEMAS and FEM5 were installed in different computers but connected through network. FEMAS was installed in Sun Workstation with

---

by Finite Element Method). Tokyo (In Japanese).

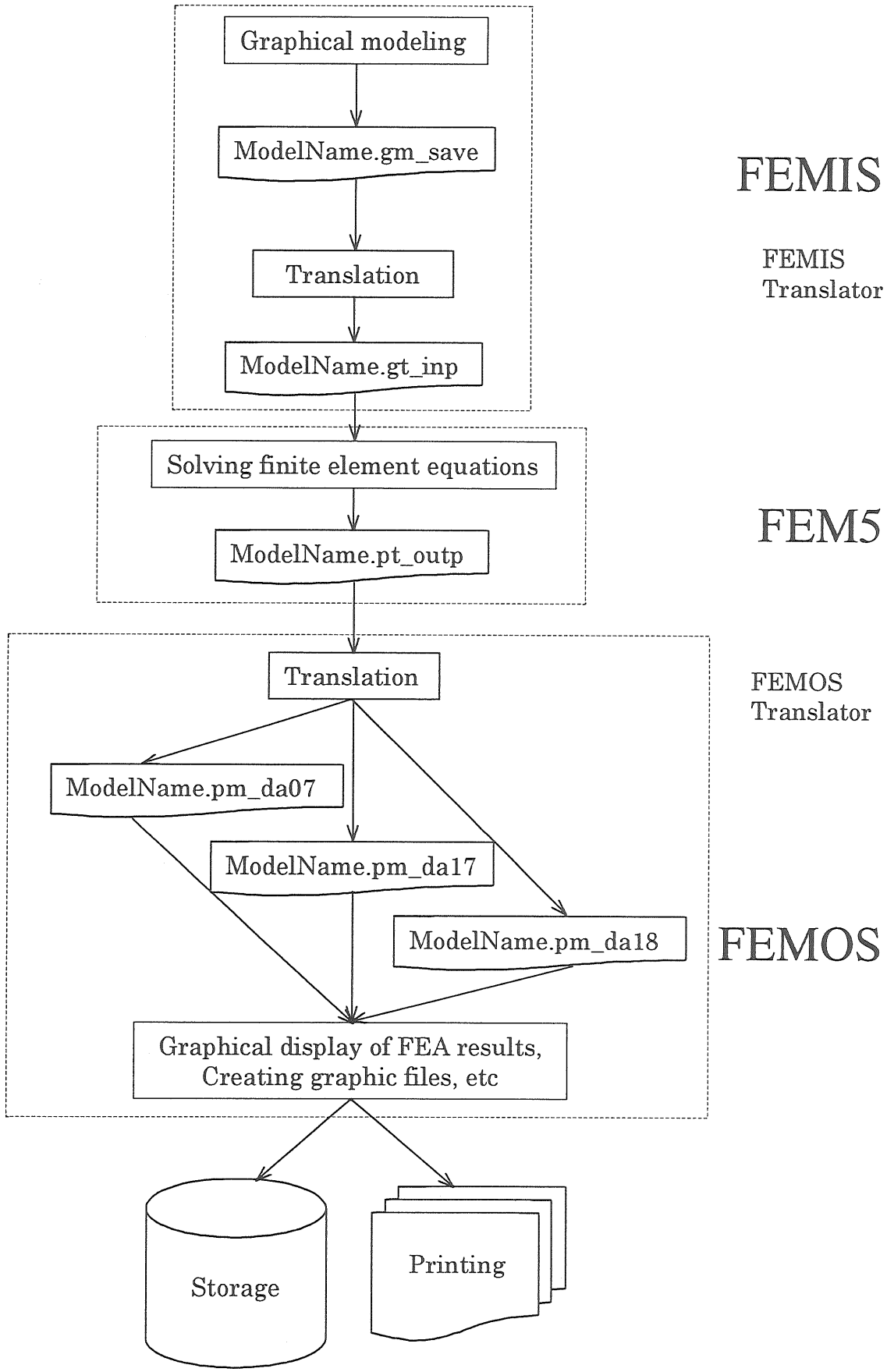

Fig. 3.1 Numerical analysis with FEM using FEMAS and FEM5.

Solaris operating system, while FEM5 run in Fujitsu VPP500/30 computer under UXP/M operating system with a maximum speed of 47 GFLOPS[*,14,15]. The use of two programs installed on separate computers proved to be inconvenient especially when a lot of error occurred. In many cases, the errors were found later after the translated FEMIS file were fed into FEM5, and correction could be done only after running FEMAS again. Another disadvantage was that not all FEM5 commands were available in FEMIS such that further editing of input file for FEM5 was inevitable[†].

(b) FEM Models

One of the problems in mass reduction using aluminum is the lack of stiffness. Thus, design of a lighter aluminum structure that effectively replaces steel must overcome its lower modulus of elasticity (64 versus 205 GPa for steel structure) by its lower density (2.8 versus 7.9 Mg/m^3 for the steel structure). Due to this big difference in modulus of elasticity, stiffness dictates member sizing more than strength. For a stiffness-based design like this frame model, the member sizing is mainly based on a general equation for beam's deflection as follows;

$$EI \frac{\partial^2 y}{\partial x^2} = M(x) \tag{3.4}$$

---

[*] Center for Science and Information Processing, University of Tsukuba. 1996. Guide to VPP500/30 Supercomputer. Tsukuba (In Japanese).

[†] Center for Science and Information Processing, University of Tsukuba. 1996. Guide to Finite Element Method with Supercomputer. Tsukuba (In Japanese).

where

I : area moment of inertia, m^4

y : deflection, m

x : horizontal distance from origin, m

M : moment, N·m

To maintain the same deflection at the same moment, then flexural stiffness, EI, should be the same. Furthermore, because aluminum has about one-third modulus of steel, then it should has about three times moment of inertia. This change could be done by changing the shape and or the size of a member.

This study was based on a commercially available 17-kW tractor with a chassis-type frame made of hollow rectangular members. Since in this first approach, it was intended to make aluminum frame without modifying member shape, the only possibility to improve moment of inertia of a member is just by changing the size. For mass reduction, moment inertia should be maximized while simultaneously minimize the cross-sectional area. The area moment of inertia and cross-sectional area of a hollow rectangular shape is given by equations (3.5), (3.6), and (3.7) while the notation is presented in Fig. 3.2.

$$I_x = 1/12\{b \cdot h^3 - (b-2t_b)(h-2t_h)^3\} \quad (3.5)$$

$$I_y = 1/12\{h \cdot b^3 - (h-2t_h)(b-2t_b)^3\} \quad (3.6)$$

$$J = 2/3(h_1 \cdot t_b^3 + h_2 \cdot t_h^3) + (2h_1^2 \cdot h_2^2 \cdot t_b \cdot t_h)/(h_1 \cdot t_h + h_2 \cdot t_b) \quad (3.7)$$

$$A = 2(h \cdot t_b + b \cdot t_h - 2t_b \cdot t_h) \tag{3.8}$$

where

I_x : area moment of inertia with respect to x-axis, m^4

I_y : area moment of inertia with respect to y-axis, m^4

J : polar moment of inertia, m^4

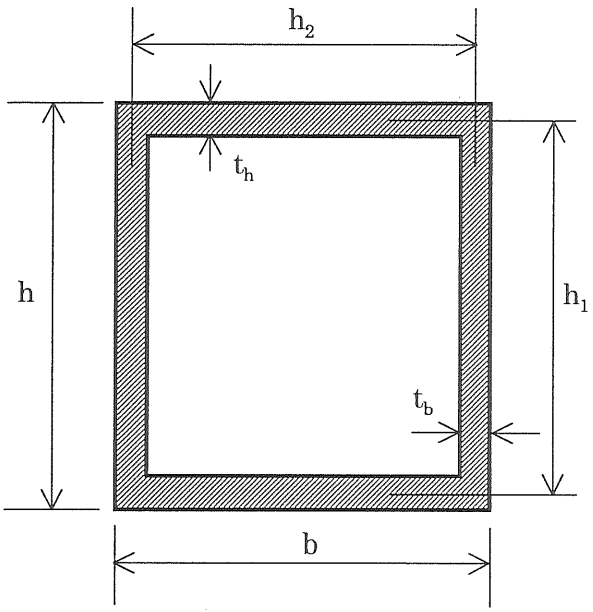

Fig. 3.2 Cross-section of a hollow rectangular member and its notation.

Although there are three kinds of moment of inertia, the most important one is I_x since it is directly related to vertical stiffness of the frame which is mainly contributed by the member individually. The value of I_y and J are related to lateral and torsional stiffness of individual member. These values are less important because frame as a whole will resist lateral and torsional load instead of individual member. In this respect, area moment of inertia of the whole frame is more pertinent. These ideas guide the size

selection of aluminum member.

Direct substitution of aluminum for steel will result in lower flexural stiffness. On the other hand, merely changing the member's size, although may retain stiffness, will likely increase its mass. Based on the equation (3.5) and (3.8), member's flexural stiffness at a given mass could be improved by increasing its outer size and simultaneously reducing its thickness.

Although this method also does apply to steel, to obtain the same mass-stiffness ratio, the thickness of the steel member must be very thin which is impractical to manufacture and require extensive rust-proofing treatment to extend its service life. The manufacturing limit for mild steel thickness is 1.14 mm. On the other hand, because aluminum is easier to be formed and resistant to corrosion, thinner aluminum tube can be manufactured. Current manufacturing limit for thickness of aluminum structural tube is 1 mm[47]. Even without referring to this manufacturing limit, aluminum can be manufactured with thickness three times to that of steel while maintaining the same mass because of its lower mass density.

Existing frame is composed of structural tube with a cross section of 100 × 40 × 3 mm (h × w × t). With scale factor of 2, the model member should have a cross section of 50 × 20 × 1.5 mm although what is commercially available was this section with 1.6 mm thickness. Considering the geometrical limitation in existing structure and the available material in the market, an aluminum member having comparable stiffness with cross-section of 60 × 30 × 2.5 mm was selected.

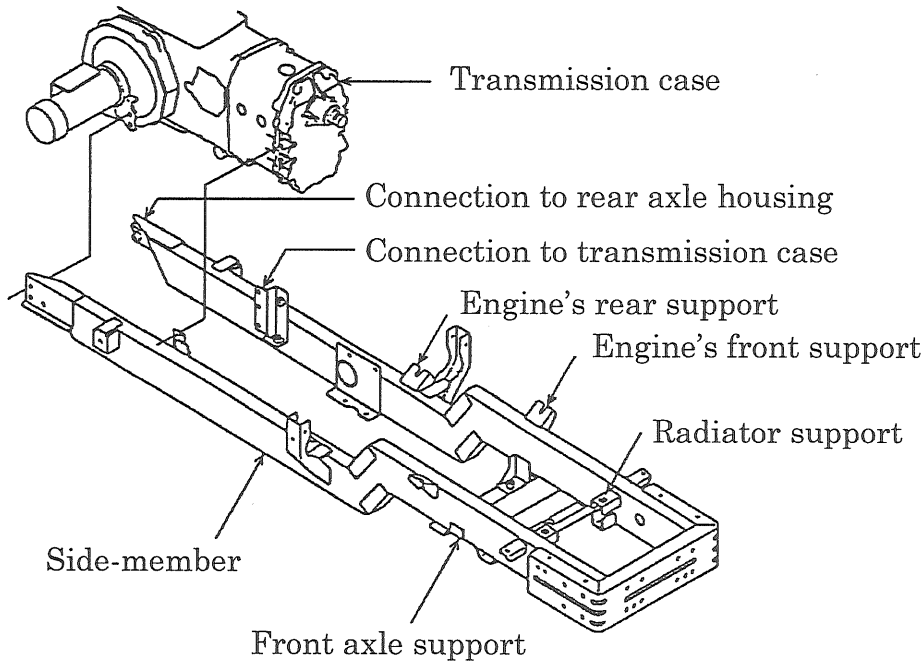

(a)

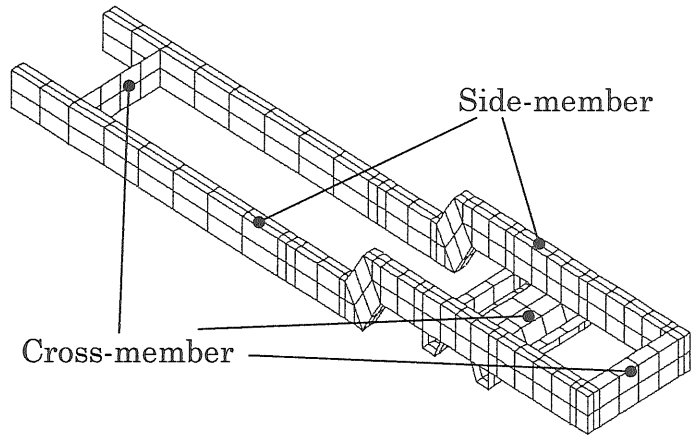

(b)

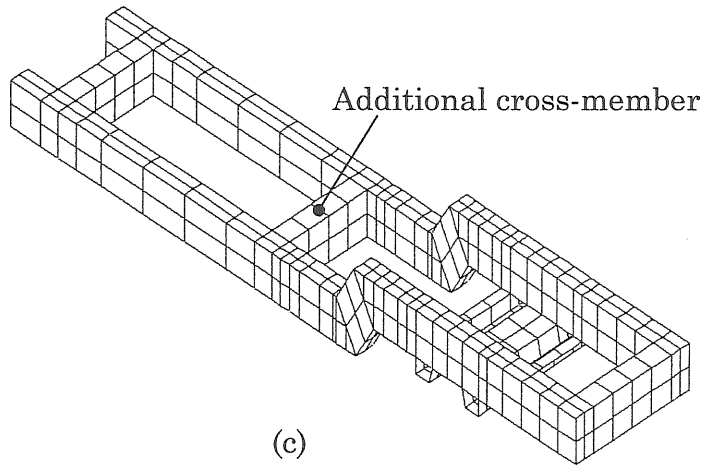

(c)

Fig. 3.3 Existing frame and its numerical models: (a) existing frame, (b) steel model, (c) aluminum model.

Thus, numerical models were made based on the selected materials and constructed by rectangular (QUADE) and triangular shell elements (TRIAE) which have five-degree-of-freedom on each node (Fig. 3.3). The steel model consisted of 616 elements and 602 nodes while the aluminum model consisted of 682 elements and 648 nodes. The figure also shows that, one additional cross-member between clutch and transmission box was introduced in the aluminum model to reinforce torsional and lateral stiffness.

(c) Applied loading

To evaluate the strength characteristics of the two models, various loading cases were applied (Fig. 3.4). The loading cases were simulated forces considering body mass, front loader, front-mount earth-moving blade, mid-mount earth-moving blade or mower, additional front mass, and lateral or torsional loading. While the first six loading cases were similar to previous study on tractor frame[51], the rest were lateral and torsional loads that represent maximum loads that the frame models could support. The magnitude of forces was scaled down according to equation (3.3).

(d) Static-Elastic Analysis

In this research, only an elastic static analysis was conducted to meet the specific research concerns. Although elastic-plastic analysis is important in characterizing frame structural strength, this was not conducted due to

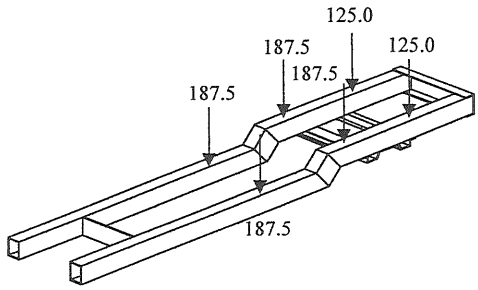

Loading case-1: Body mass

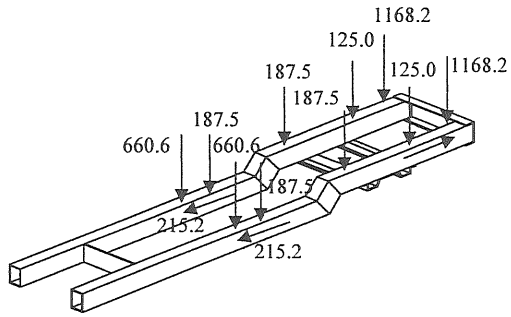

Loading case-2: Front loader

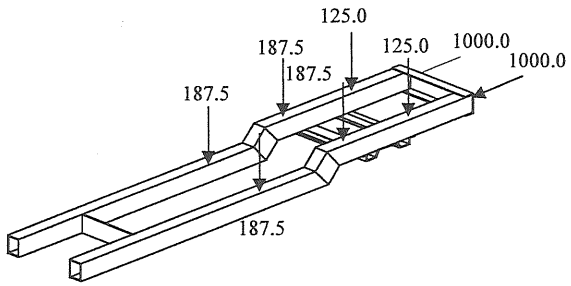

Loading case-3:
Front-mount earth-moving blade

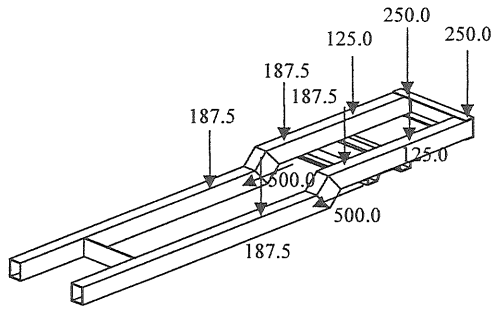

Loading case-4:
Mid-mount earth-moving blade

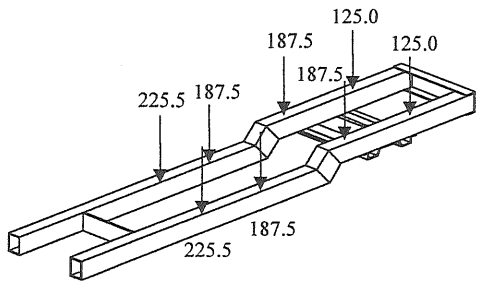

Loading case-5:
Mid-mount mower

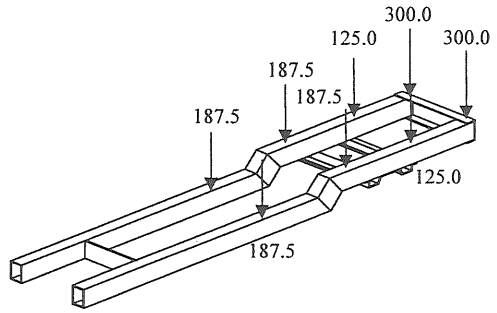

Loading case-6:
Additional mass

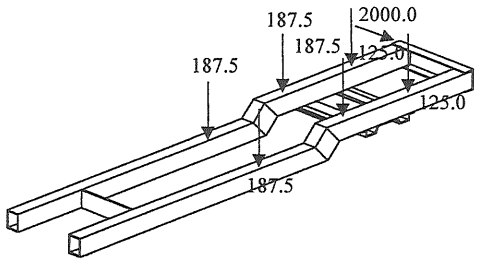

Loading case-7: Lateral loading

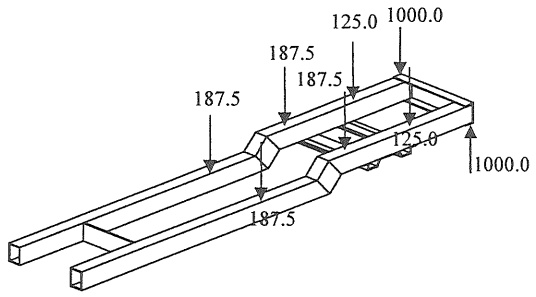

Loading case-8: Torsional loading

Fig. 3. 4 Direction and magnitude of external forces in loading case-1 to 8. Digits denote forces in newton.

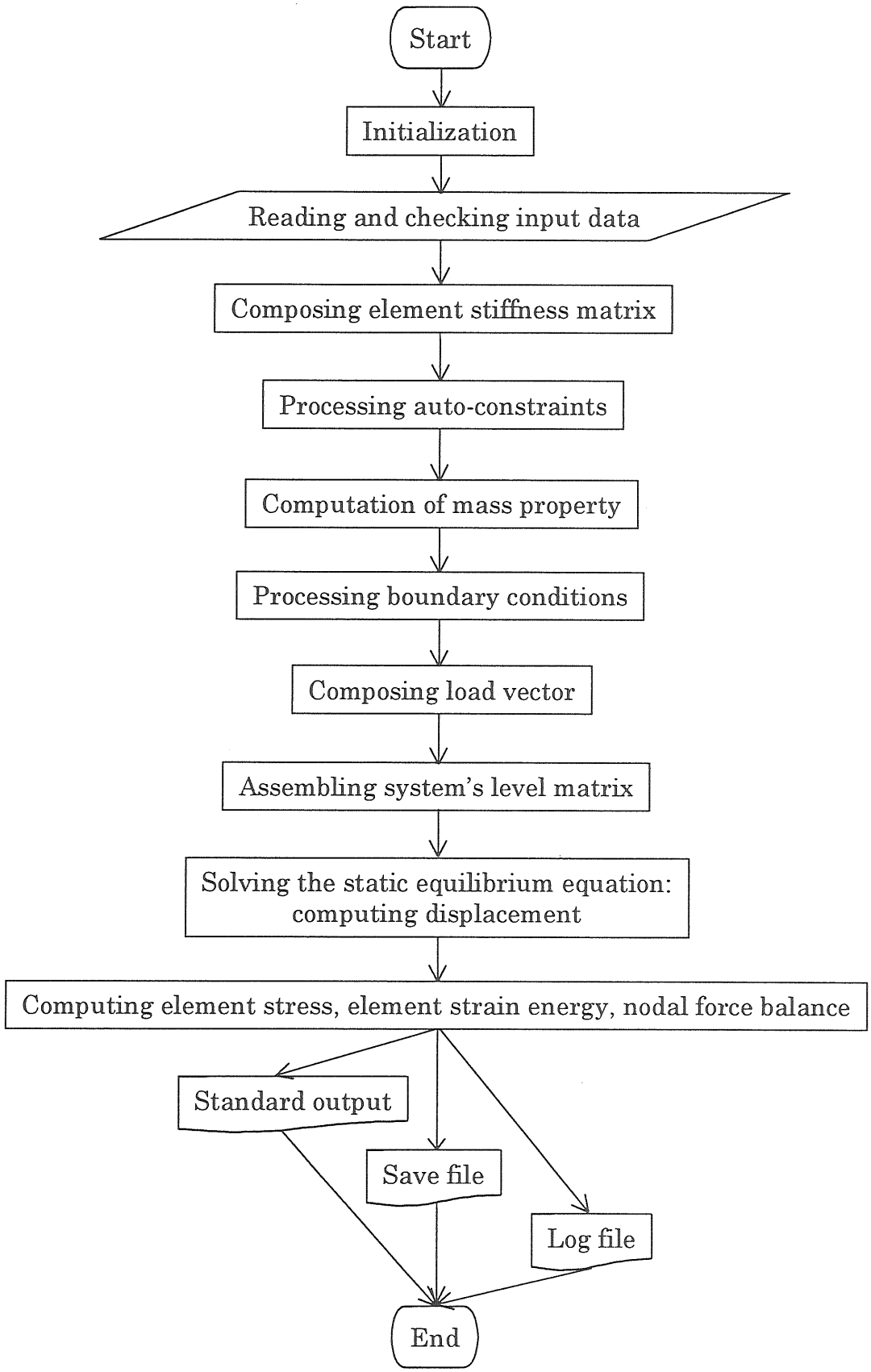

Fig. 3.5 Outline of static analysis with FEM5.

unavailability of related module in the FEM5 program and the fact that this type of analysis has been done by other researcher[24].

Process of static elastic analysis by using FEM5 is given in Fig. 3.5. Calculation started with composing element stiffness matrix. After furnishing it with loading and constraints, FEM5 assembled the equation in system level, and then solved the static equilibrium equation. For linear static analysis, the equation is as follows[*, 67]:

$$\{K\}\ \{U\} = \{R\} \tag{3.9}$$

where

K : system stiffness matrix

R : load vector

U : displacement vector

Since K and R were known, solution produced nodal displacement. From this, then reaction force, element stress, and element strain energy were computed. Von Mises, combined displacement etc. were computed later by FEMOS.

Based on the results regarding stresses, the structural strength of the aluminum and steel model was compared. In this evaluation, the von Mises yield criterion was taken into account. Compared to other failure theory, Mises yield theory was known of having best agreement with actual

[*] Fujitsu Company. POPLAS®/FEM5 Manual for V25.

measurement in experiment using ductile materials like steel and aluminum[53), 65)]. The von Mises equivalent stress, σ_m, is defined by:

$$\sigma_m = \frac{1}{2}\sqrt{(\sigma_1 - \sigma_2)^2 + (\sigma_2 - \sigma_3)^2 + (\sigma_3 - \sigma_1)^2} \tag{3.10}$$

where σ_1, σ_2, and σ_3 are principal stresses.

One disadvantage of aluminum is its lower stiffness compared to steel. In this study, the structural stiffness of the two model was evaluated using maximum deflections under a given loading.

3.2.3 Loading tests

(a) Experimental models

Both steel and aluminum experimental frame models were fabricated using mainly bolts for joining each member (Appendix A). Groove welding was applied for connecting the parts of side-members. The material used for steel structure was JIS STKR 400 while that for aluminum structure was 6061-T6. Although the two models have the same length at 975 mm, the aluminum model was wider at 193.5 mm than that of steel (173.5 mm). The properties of these two materials are listed in Table 3.1. The same property was also used in FEM analysis.

(b) Procedure of loading tests

Fig. 3.6 depicts the schematic diagram of loading tests. In these tests, several selected vertical loads were applied to the models by using ballast with known mass in order to facilitate precise measurement. Two loading

Table 3.1 Material property of frame models

Property	Mild steel[2,7]	Aluminum alloy[1]
Young's modulus, GPa	205	63.8
Yield stress, MPa	257	255
Tensile strength, MPa	400	310
Poisson's ratio	0.30	0.33
Density, Mg/m^3	7.8	2.79

tests were conducted: loading test-1 and loading test-2. Loading test-1 represented very simple loading in the center of the frame as shown in Fig. 3.6. Applied load were 196N, 373 N, 746 N, and 1196 N. In the loading test-2, force of 115 N was simultaneously applied at points I, J, K, L, M, and N.

Strains were measured using temperature compensated, three-element rectangular rosette strain gages and recorded by a personal computer through three Kyowa PCD-100A sensor interface boards having 12 channels. Since each rosette was composed of three gages, the maximum number of locations which could be covered in a simultaneous measurement were four (A, B, C, and D). Data stored in the computer can be read directly by spread-sheet program by which further data processing was performed.

Deflections were measured with a Keyence laser displacement sensor LK-080 at supporting points (E and I) and at selected points on the frame members (F, G, H, and J). The output voltage was displayed through a Metex digital multimeter M-3870D and then converted into deflections by using a calibration equation supplied by the manufacturer. Unlike stress

measurement, deflection could be measured only at one location in each experiment due to limited number of sensors. Thus, for six locations of one loading, six runs had to be conducted.

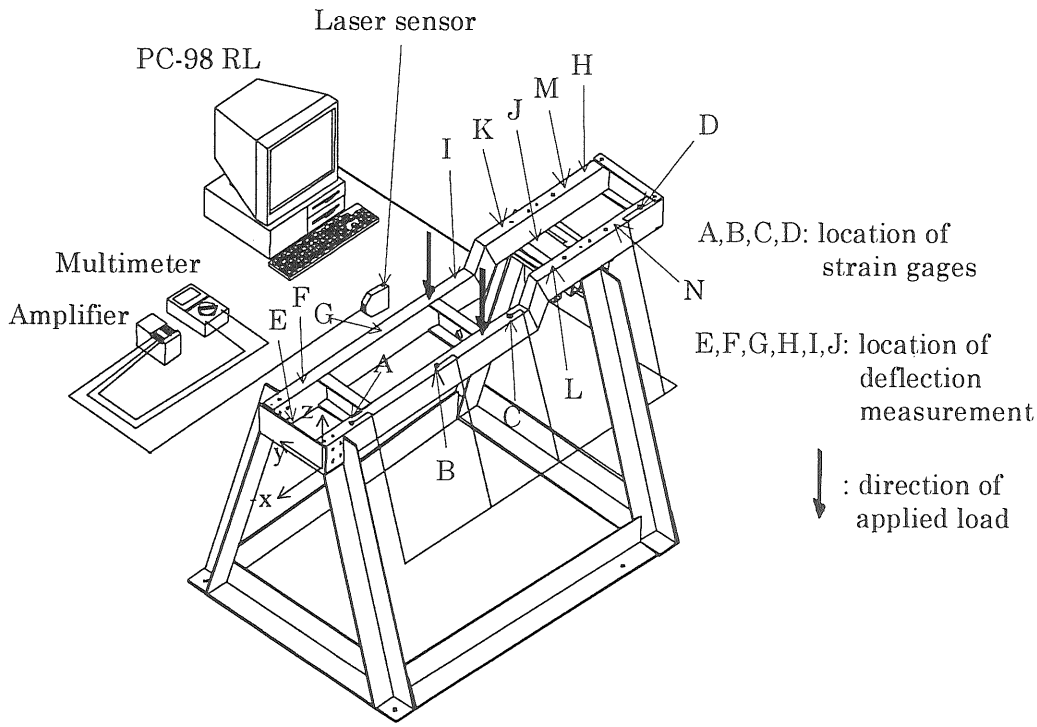

Fig. 3.6 Loading test set-up.

(c) Calculation of stress from measured strain

Three-element rectangular strain gage simultaneously measured strain in three directions: 1, 2 and 3 (Fig. 3.7). If the true strain from at those directions are ε_1, ε_2, and ε_3, respectively, then the maximum (ε_{max}) and minimum strain (ε_{min}) are as follows[14]:

$$\varepsilon_{max} = \frac{1}{2}(\varepsilon_1 + \varepsilon_2) + \frac{1}{\sqrt{2}}\sqrt{(\varepsilon_1 - \varepsilon_2)^2 + (\varepsilon_2 - \varepsilon_3)} \qquad (3.11)$$

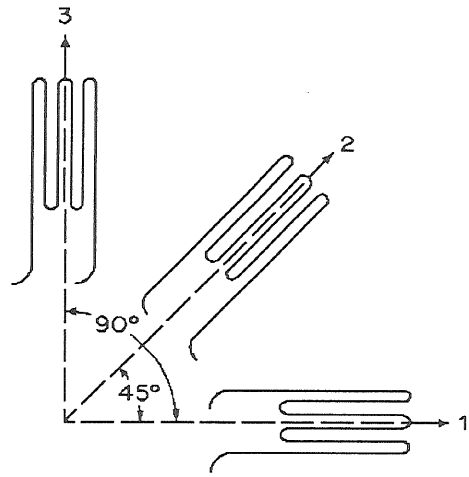

Fig. 3.7 Three-element rectangular rosette gage

$$\varepsilon_{min} = \tfrac{1}{2}(\varepsilon_1 + \varepsilon_2) - \tfrac{1}{\sqrt{2}}\sqrt{(\varepsilon_1 - \varepsilon_2)^2 + (\varepsilon_2 - \varepsilon_3)} \tag{3.12}$$

Based on maximum and minimum strain, the following formulas give the value of maximum and minimum stress, σ_1 and σ_3[14, 58]:

$$\sigma_1 = \frac{E}{1-\mu^2}(\varepsilon_{max} + \mu\varepsilon_{min}) \tag{3.13}$$

$$\sigma_3 = \frac{E}{1-\mu^2}(\varepsilon_{min} + \mu\varepsilon_{max}) \tag{3.14}$$

Readings taken from individual gages of a three-element rectangular rosette, however, are not true strains. If T is the coefficient of transverse sensitivity of the strain gage, the relationships between the true strains and the readings from the gages (Q_1, Q_2, Q_3) are given by:

$$\varepsilon_1 = Q_1 - TQ_3 \tag{3.15}$$

$$\varepsilon_2 = (1 + T)Q_2 - T(Q_1 + Q_3) \tag{3.16}$$

$$\varepsilon_3 = Q_3 - TQ_1 \tag{3.17}$$

By substituting equations (3.15), (3.16), and (3.17) into equations (3.11), and (3.12), then these two equations into equation (3.13) and (3.14), the principal stresses appear as functions of the three strain-gage readings[21].

$$\sigma_1 = \frac{E(1-T)}{2(1-\mu)}(Q_1+Q_2) + \frac{E(1+T)}{\sqrt{2}(1+\mu)}\sqrt{(Q_1-Q_2)^2+(Q_2-Q_3)^2} \tag{3.18}$$

$$\sigma_3 = \frac{E(1-T)}{2(1-\mu)}(Q_1+Q_2) - \frac{E(1+T)}{\sqrt{2}(1+\mu)}\sqrt{(Q_1-Q_2)^2+(Q_2-Q_3)^2} \tag{3.19}$$

3.3 Results and discussion

3.3.1 Strength and stiffness analysis by FEM

Selected parts of input file for and output file from FEM5 program are presented in Appendix B and C. The results of FEM on maximum von Mises stress that occurred in each loading case are given in Fig. 3.8. According to equation (3.3), these stresses were similar to the stresses that occurred in prototypes such that the results can be directly applied to prototypes. Fig. 3.8 shows that considerable stress reduction was achieved by replacing the steel model with the aluminum model since the stress levels of aluminum were roughly 24 to 54% lower than that of steel.

For practical comparison, this stress value can be compared to its allowable stress that represents the condition of maximum loading in a conservative design. For example, in loading case-2, the maximum stress for

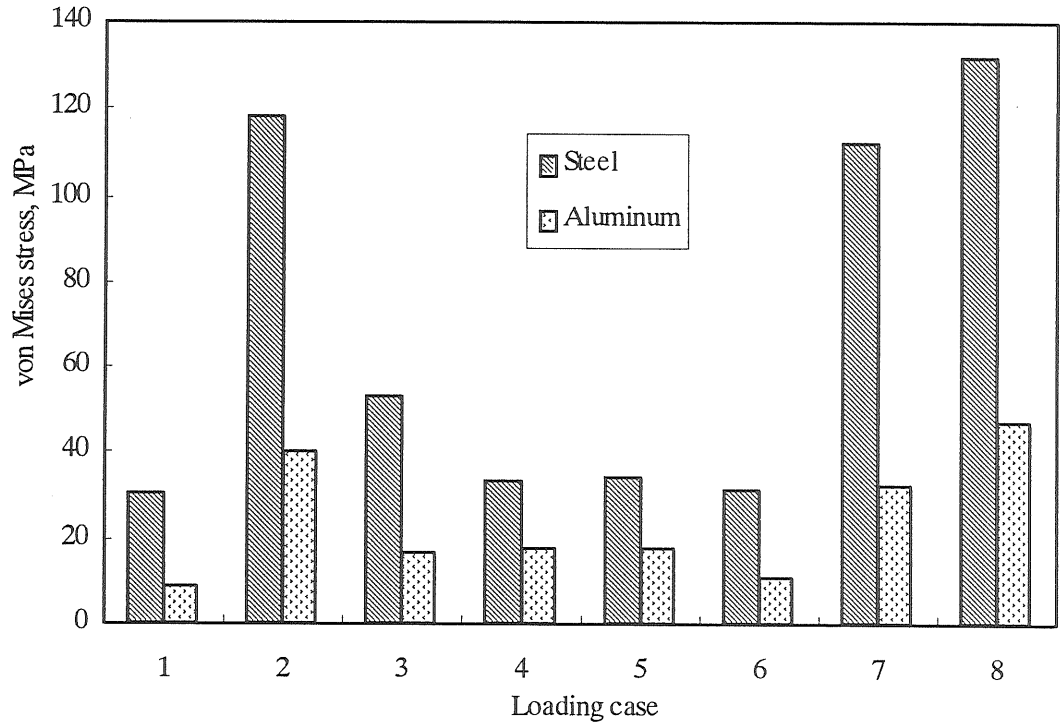

Fig. 3.8 Maximum von Mises stress in each loading case.

steel model was 118.0 MPa. This was 91% of the allowable stress of 130 MPa at safety factor of 3. On the other hand, at the same safety factor, the corresponding value in aluminum model was only about 39% of its allowable stress. Based on these findings, the load on the aluminum model could be increased by as much as 2.5 times before maximum allowable stress is reached, unlike that of steel model which could be increased only by 10%. Similar trends were found in other loading cases. These results indicated that, by using aluminum frame, the numerical stress not only decreased but the relative strength of the frame structure also improved. The reason of this was an increase in member section of 20% in height, 50% in width, and 56% in thickness. The load carrying capacity of the structure in the elastic

range roughly increased by about two folds. This increase in load carrying capacity implies that the aluminum model can give better safety for field operation as well as greater flexibility in designing or styling of tractors.

As shown in Fig. 3.8, high stresses occurred in loading cases-2, -7 and -8. Stress distributions in the steel and aluminum models for loading case-2 are shown in Fig. 3.9. For the steel model, stresses in the front section of the member were generally higher than that at the rear. Maximum stress of 98.9 MPa at node number 457 and 462 occurred on the bottom side of cross-member R which connects to front axle. Additional stress took place on the top-side of front member, *e.g.,* T and U (Fig. 3.9(a)) with maximum stress at about 90 MPa. However, in the remaining portions, particularly at cross-member P, Q and S, stresses were saliently low for all six loading cases because external loads were applied parallel to the x- or z-direction.

A similar pattern also occurred in the aluminum model. Maximum stress, in terms of von Mises stress of 43 MPa, occurred at node number 509 and 527, which were similar in location with that of steel model. However, while the locations of higher stresses in the side-member of the steel model coincided in the middle part of the member (T and U), high stresses in the aluminum model occurred in the inner side of the member (V and W) as shown in Fig. 3.9.(b). This was because of higher stiffness of the aluminum model's cross-member.

As stated earlier for loading cases-1 to -6, stresses in cross-members were always low due to the nature of the loads. Dissimilar to loading cases-1

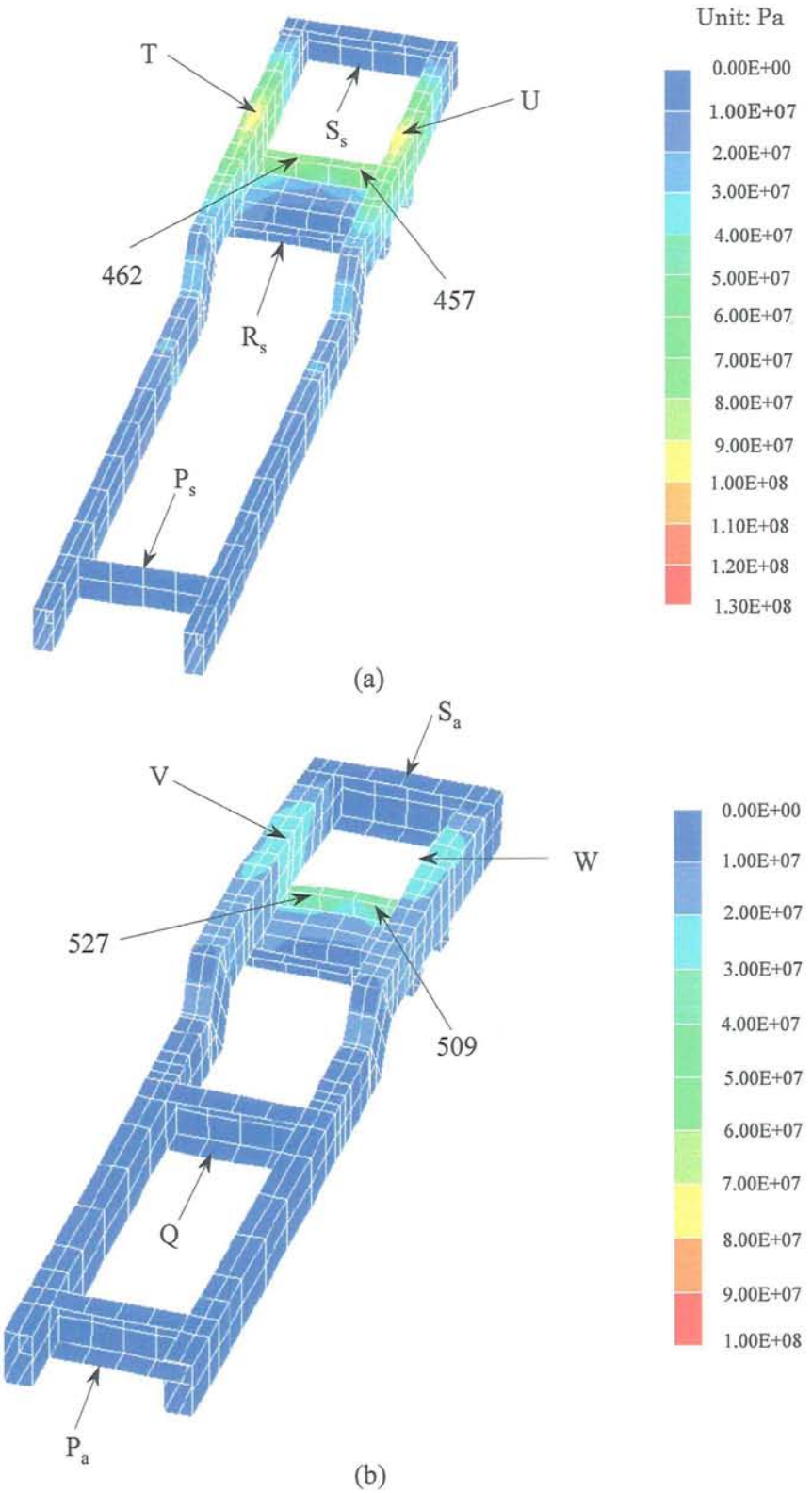

Fig. 3.9 Stress distribution under loading case-2: (a) steel model (b) aluminum model. Digits denote node numbers.

to -6 which mainly dealt with the role of side-member in resisting vertical and longitudinal forces, loading cases-7 and -8 revealed the role of cross-member in resisting lateral and torsional loading. The distribution of stresses in the two models under loading case-7 is given in Fig. 3.10. In this loading, the role of rear and middle cross-member (P and Q) can be seen by the increase in stress levels in these portions. Since both members carried the load, the value of stress increased considerably compared to previous six loading cases. For steel model, maximum stress due to lateral loading occurred at node 293 and 303. Another critical node was node 7, located in welded joint, which has weaker mechanical resistance.

In the aluminum model, the introduction of middle cross-member Q caused higher stresses near the connection of cross- to side-member, especially in nodes 169 and 186. Similar to the steel model, high stress also occurred near rear axle connection at node 40 but at a safer distance of 5 cm away from the joint.

In torsional loading (Fig. 3.11), stresses in frame members were more evenly distributed than in other loadings. Nonetheless, the stresses in cross-members in the two models were still relatively low. Maximum stress in the steel model occurred at node 208 while this took place at node 258 for the aluminum model, which is similar in location with that in steel model.

In general, the stress distributions of the two frame models in the three previous loading cases were similar. This also holds true for the remaining loading cases. Even when the loads were increased up to yield points, this

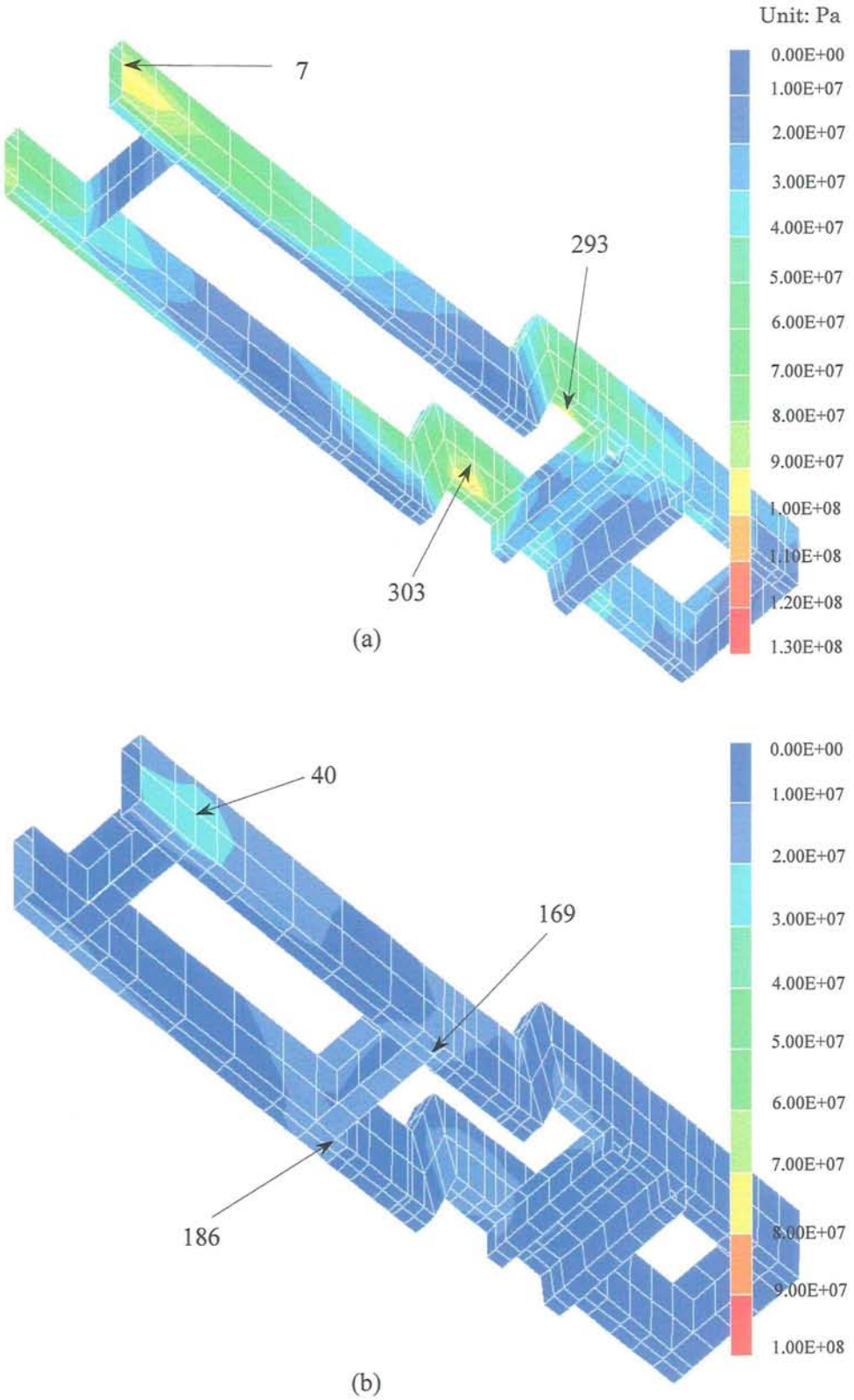

Fig. 3.10 Stress distribution under loading case-7: (a) steel model (b) aluminum model. Digits denote node numbers.

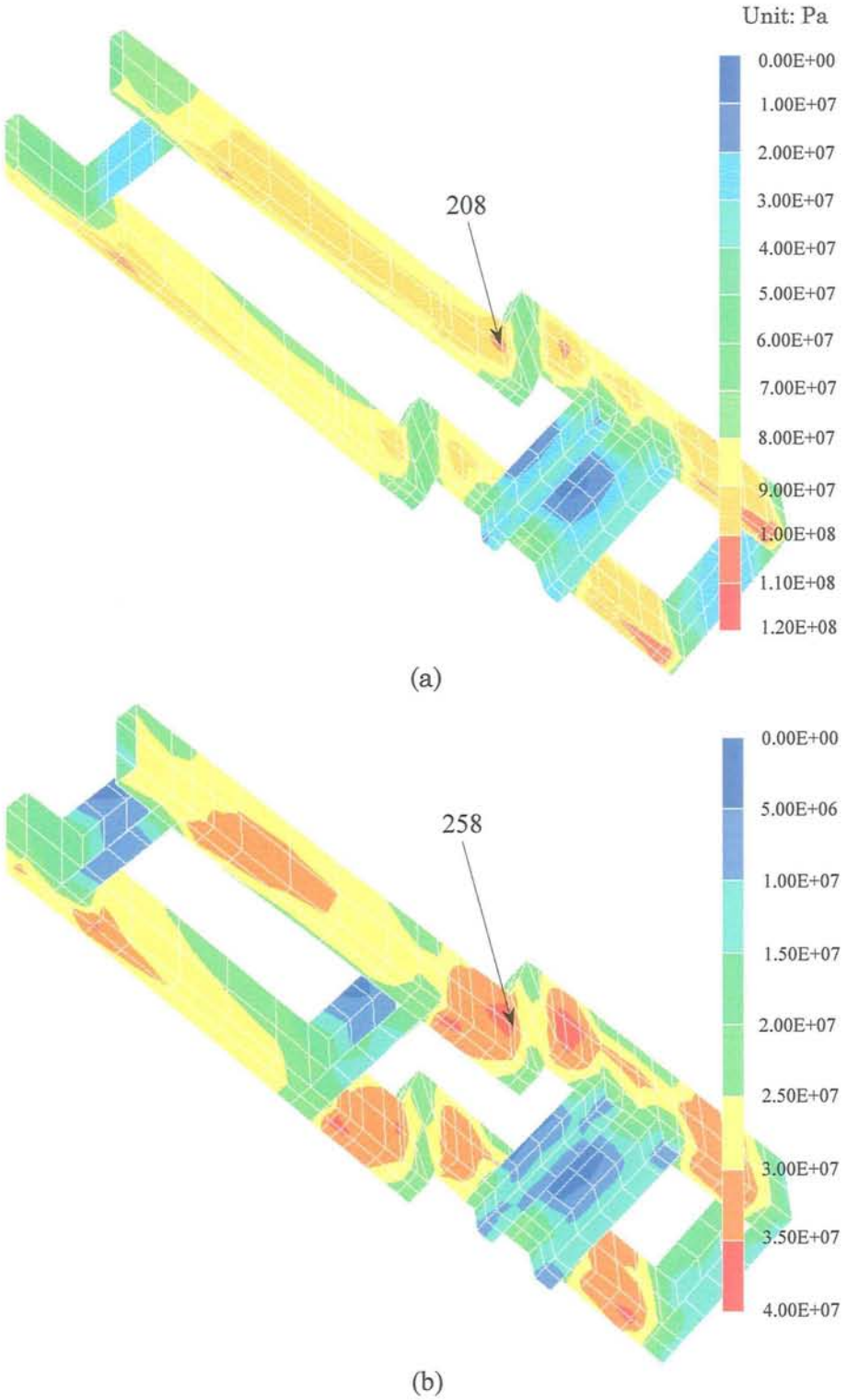

Fig. 3.11 Stress distribution under loading case-8: (a) steel model (b) aluminum model. Digits denote node numbers.

condition remained the same since the two frames have similar configuration.

In order to minimize the detrimental effects of vibration, the tractor structure requires high stiffness. Thus, attention should be given also to the stiffness or rigidity of the structure which may be evaluated through its load-deflection relationship. The lower the deflection, the more rigid the structure becomes. Although the aluminum structure showed higher strength for loading cases-1 to -6 (Table 3.2), its deflection in z-direction was always higher than that of steel. In this direction, the aluminum frame has 12% less rigidity than the steel frame. For loading cases-7 and -8, the results were opposite in that the aluminum model was stiffer than the steel one. Due to additional U-shaped cross-member in the middle part of the frame, aluminum structure was 60% and 33% stiffer than steel structure for lateral and torsional loading, respectively.

The fact that the aluminum model has less rigidity in the vertical direction may affect its characteristics under dynamic conditions. Because natural frequency is inversely proportional to the square root of maximum deflection, it can be predicted that the aluminum model will have a slightly lower natural frequency. Although more computations are needed to find the exact value, for greater comfort, a higher natural frequency is usually better since it will not interact with terrain-induced excitation which has a frequency of 1-10 Hz[47]. This topic will be examined in the next chapter.

Table 3.2 Maximum deflection in loading case-1 to 8 ($\times 10^{-6}$ m)

Model	Loading case							
	1	2	3	4	5	6	7	8
Steel								
x	-8	113	-53	-35	28	-16	324	136
y	-7	25	12	7	10	7	1 622	-5 214
z	-49	-561	-160	146	148	-102	-3 516	-284
Aluminum								
x	-9	131	-60	-41	35	-18	244	126
y	-7	34	9	9	14	8	1 527	-2 186
z	-55	-625	-183	-174	-153	-114	-2 418	-284

3.3.2 Comparison of results from FEM and measurement on loading tests

The results of stress measurements with loading test-1 at point C on steel and aluminum frames are given in Figs. 3.12 and 3.13, respectively. In terms of minimum stress, the trends in the steel structure were the same for both FEM and the actual experiments. However, the calculated values were lower by 12–36% than actual measurements. A similar trend also occurred in the aluminum model, in which FEM underestimated stresses by 10–30%.

Fig. 3.14 shows the calculated and measured stresses at points A, B, C and D under loading case-2 in the steel model. Results at points A, B, and D were similar to results in loading test-1, that is, the calculated values were somewhat lower than the measured ones. For point C, however, the calculated value was higher. The differences between calculated and measured values were about 13 to 34%.

Calculated and measured deflections at location G on both frames are

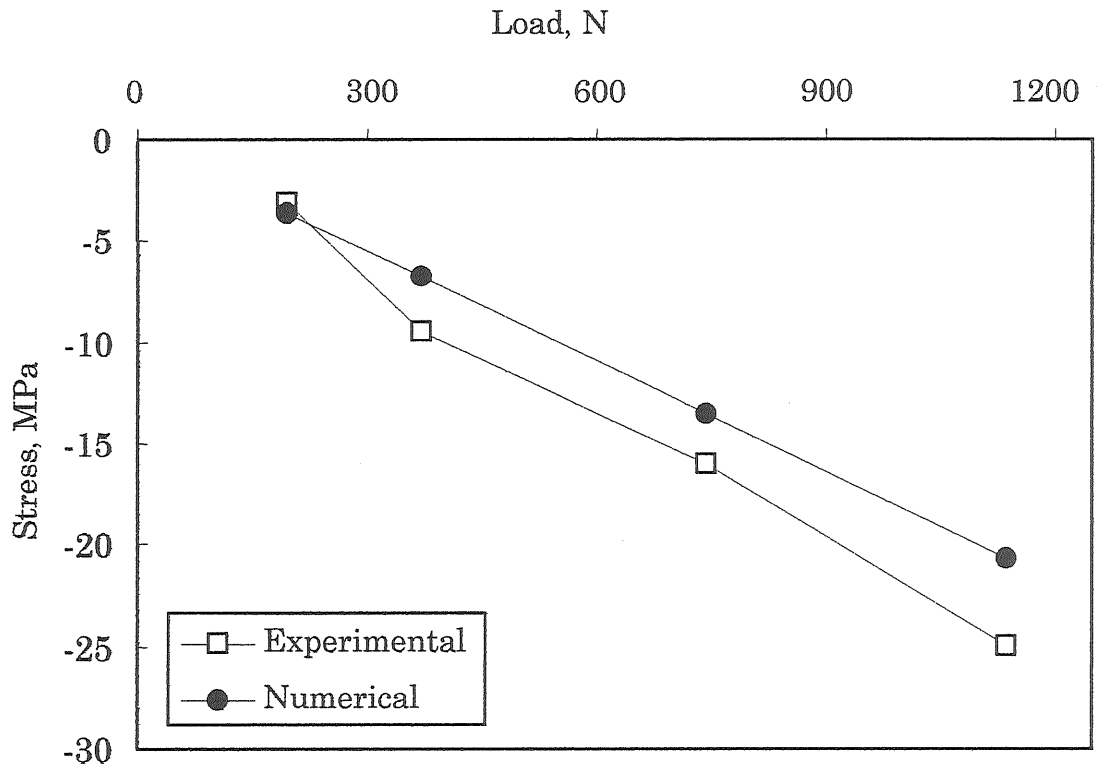

Fig. 3.12 Calculated and measured stress at C in steel model with loading test-1.

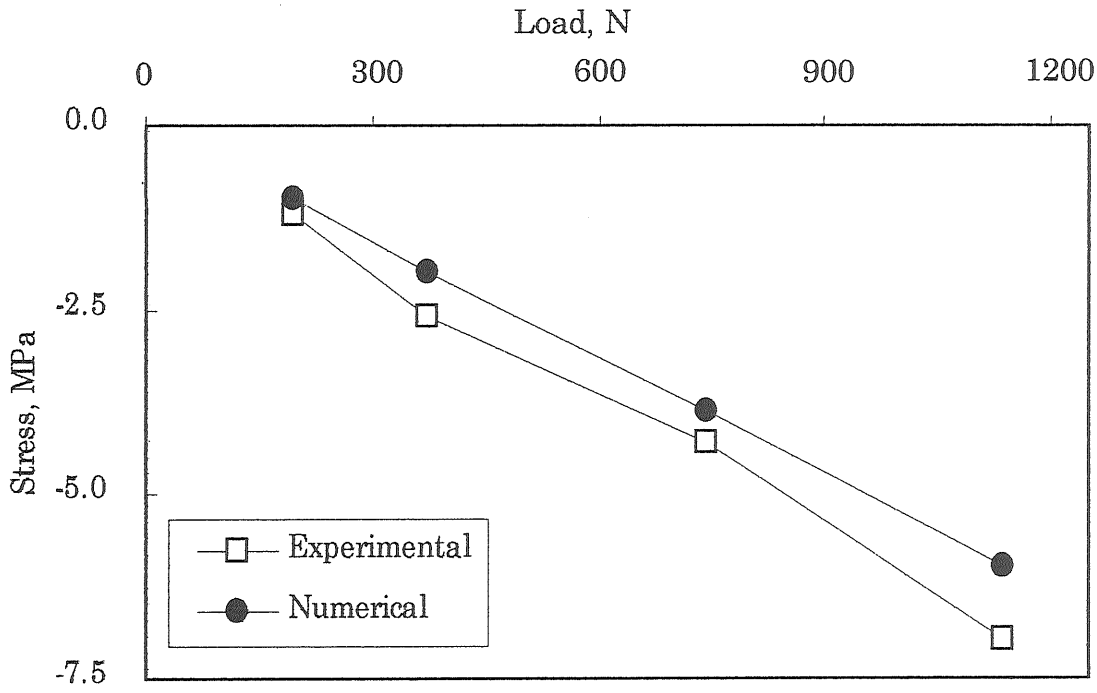

Fig. 3.13 Calculated and measured stress C in aluminum model with loading test-1.

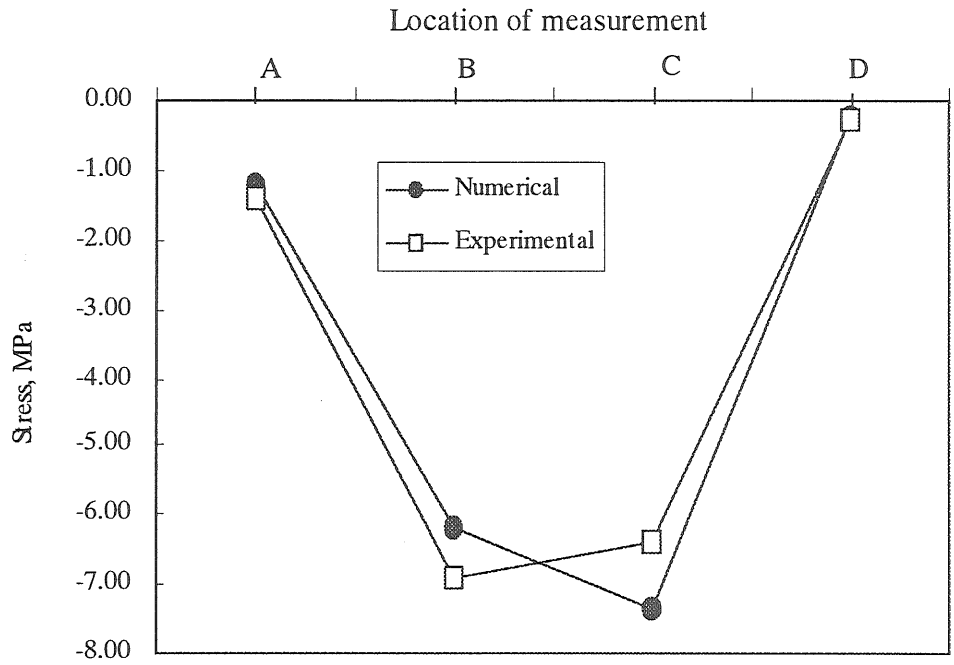

Fig. 3.14 Calculated and measured stress at A, B, C, and D in steel model with loading test-2.

presented in Figs. 3.15 and 3.16. Just like in stress measurements, FEM underestimated deflection on both frames. For steel, FEM results were 20 to 36% lower than actual measurements.

Some factors could account for the differences in the results between the FEM and loading tests. In the FEM model, it was assumed that material properties were the same at any point in the structure, which was not exactly true for the experimental models due to mechanical and thermal treatments during fabrication. Another factor that might have been contributed to this was the use of bolts for joining members. Holes for bolts and clamping force could change stress distribution around the bolted connection. Both welding and bolts effects were considered during strain

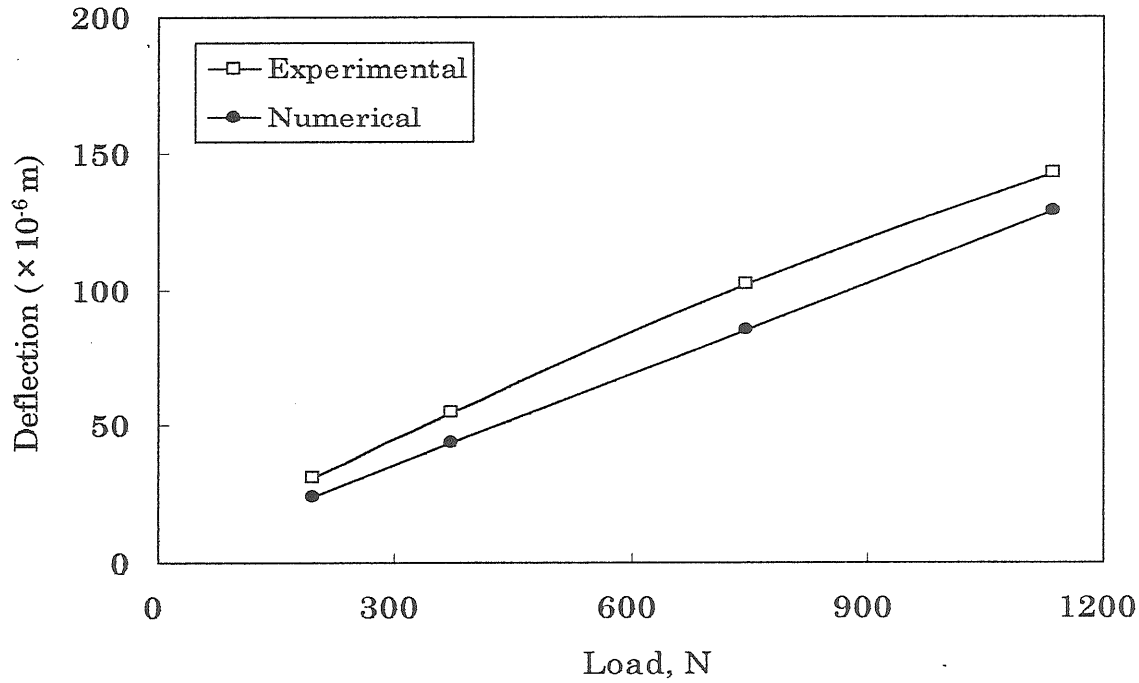

Fig. 3.15 Calculated and measured deflection at C on steel model with loading test-1.

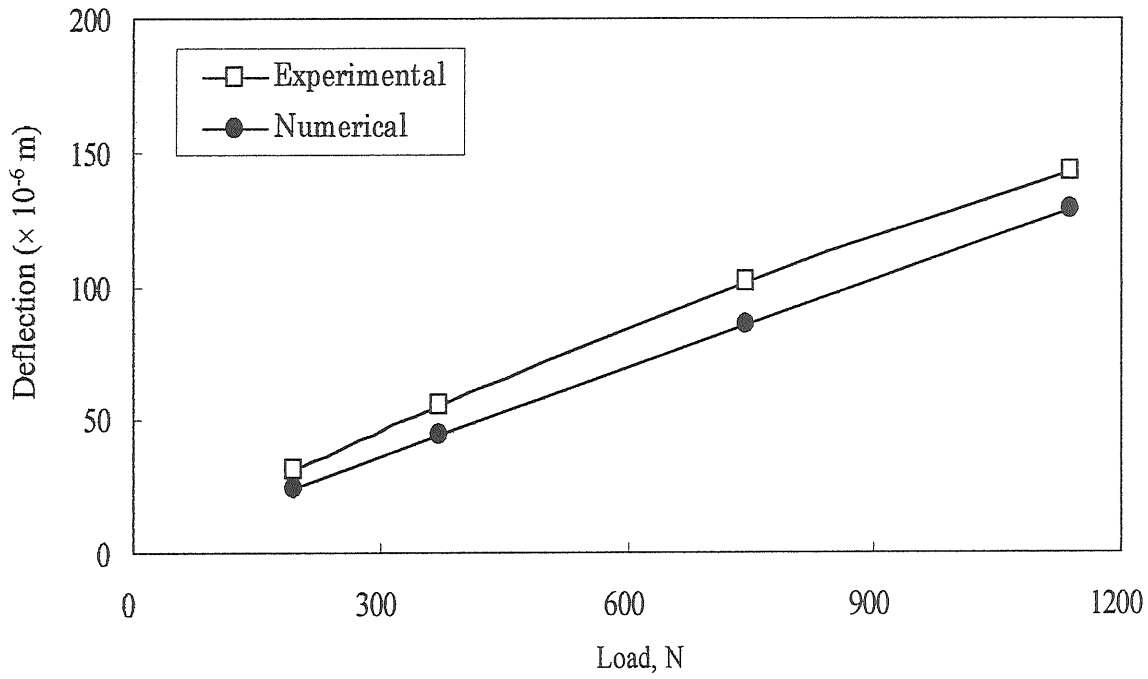

Fig. 3.16 Calculated and measured deflection at C in aluminum model with loading test-1.

gage placement and all of the gages were placed at locations far from those portions. Nevertheless, since the model was small some effects might have still existed. Another possible source of error was temperature difference. Although temperature-compensated strain gages with three-wire system were used, variation due to temperature changes

Based on these considerations, differences between FEM results and loading test results were inevitable, and thus can be accepted at this stage of study. With this, then, the previous FEM results can be considered as reflecting the true condition occurring in the two models. Although experiments with other loadings were not conducted, it can be expected that frame will also behave with reasonable agreement to the numerical analysis under such loadings.

3.3.3 Effects of aluminum substitution on mass reduction

The FEM models predicted that the mass of the steel and aluminum models were 4.2 and 3.2 kg, respectively. This means that a mass reduction of 24 % may be achieved. However, direct measurements on fabricated models revealed slightly different results, in which the steel model showed a mass of 4.0 kg while the aluminum model has 3.2 kg. According to equation (3.3), this corresponds to prototypes with mass of 32 kg and 25.6 kg for steel and aluminum, respectively, with mass reduction of only 20%.

As stated earlier, at 20% mass reduction, the aluminum model was roughly twice stronger than the steel. Thus, if the aluminum model was

made with similar strength level as the steel and design is solely based on strength, then mass reduction for aluminum model could actually reach up to 40-50%. This reduction is similar to a previous study which stated that, for square tubular sections, mass saving can be increased to 46% if the section is 40% larger[51]. In this study, this value could not be attained because of geometrical limitations in adapting to existing tractor and the limited section size available in the market. If the whole system is redesigned and the member size can be freely determined, then mass reduction may be higher.

With the present model, mass could be further reduced by removing some element in cross-members P, Q, and S. It seems this removal will not impair strength because current model has far higher lateral and torsional stiffness, and stresses in those portions are only in the order of 10-20 MPa.

3.4 Summary

Aluminum has been used to substitute steel on a tractor frame model. Numerical analysis with FEM showed that aluminum model, which was 20% lighter, has considerably higher strength than that of steel. Nonetheless, in terms of stiffness, steel model was slightly better. The analysis also showed that for strength based design, mass reduction may be attained up to 50%. For stiffness based design, however, mass reduction was far lower. Moreover, the loading test results had showed agreement with that of FEM, thus, confirmed the validity of FEM program used in this study.

Chapter 4

Further design improvement of an aluminum frame

4.1 Introduction

The first aluminum model in previous chapter showed that for strength based design aluminum gives good capability for mass reduction even without modifying the main features of existing design. Nevertheless, the model also showed its relatively lower stiffness compared to the steel model. This shortcoming can only be overcome by redesigning main members of the frame.

During field operation, tractor frame is subjected to various dynamic external loads. In such a condition, natural frequency of a structure determines the behavior of the structure in response to the external load. Furthermore, since mass and stiffness determine natural frequency of any structure, theoretically substitution of steel with aluminum will likely bring about a change in natural frequency of the structure. If the natural frequency changes, then it may be necessary to modify other tractor components to retain or improve the dynamic characteristic of the tractor. This, of course, will complicate the mass reduction effort. Therefore, it is necessary to find out the influence of this mass reduction effort on natural frequencies of the frame.

The specific objective of this chapter were

1) To further reduce the frame's mass and simultaneously increase its

stiffness by modifying the shape of frame and minimizing its mass. The evaluation of structural characteristics was conducted using FEM.

2) To find out the effect of mass reduction effort by structural modification on natural frequency of the frame.

4.2 Methodology

4.2.1 Development of FEM models

Development of FEM model was based on the total available space for chassis in the existing tractor, equal strength and stiffness to the steel model and simple manufacturing process. Fig. 4.1 shows the schematic view of the space allocation for the frame of tractor used in this study and the steel model developed in preceding chapter. The steel model was going to serve as reference for strength and stiffness during the development of finite element model for a new aluminum frame.

Development of the FEM model was conducted in two steps: side member development and whole frame development. Naturally, it was started with side member development. When the desired side member model had been obtained, then it was used to develop initial frame model.

Learning from the experience with the first aluminum model, the development of the side-member model was based mostly on the criterion of structural stiffness. Structural stiffness may be increased by selecting a sectional shape that maximizes its moment of inertia at a proper size. As moment of inertia increases in cubic proportion to the member's height, the

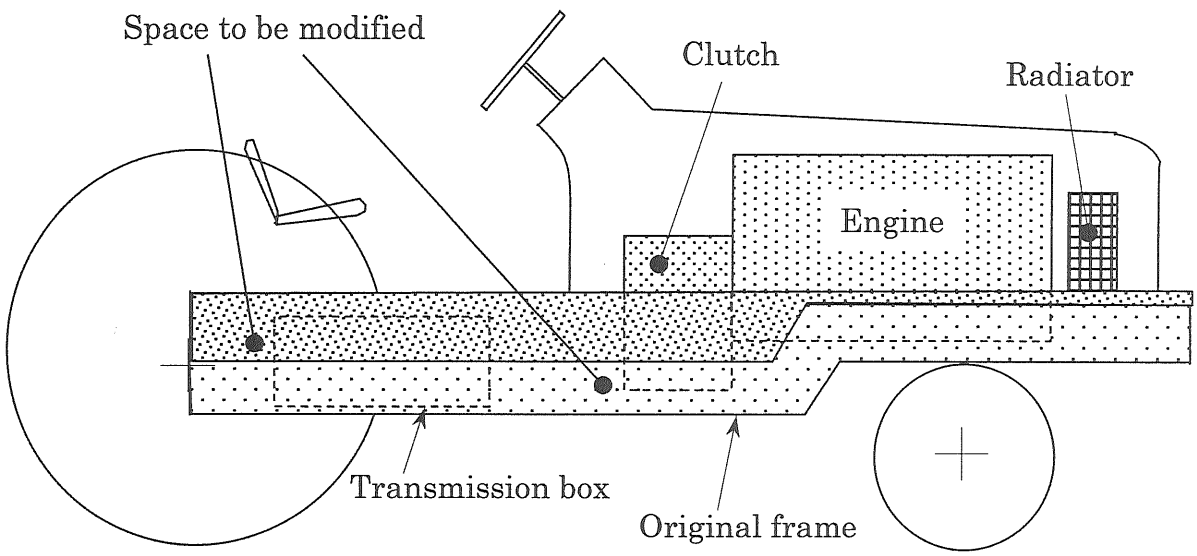

(a)

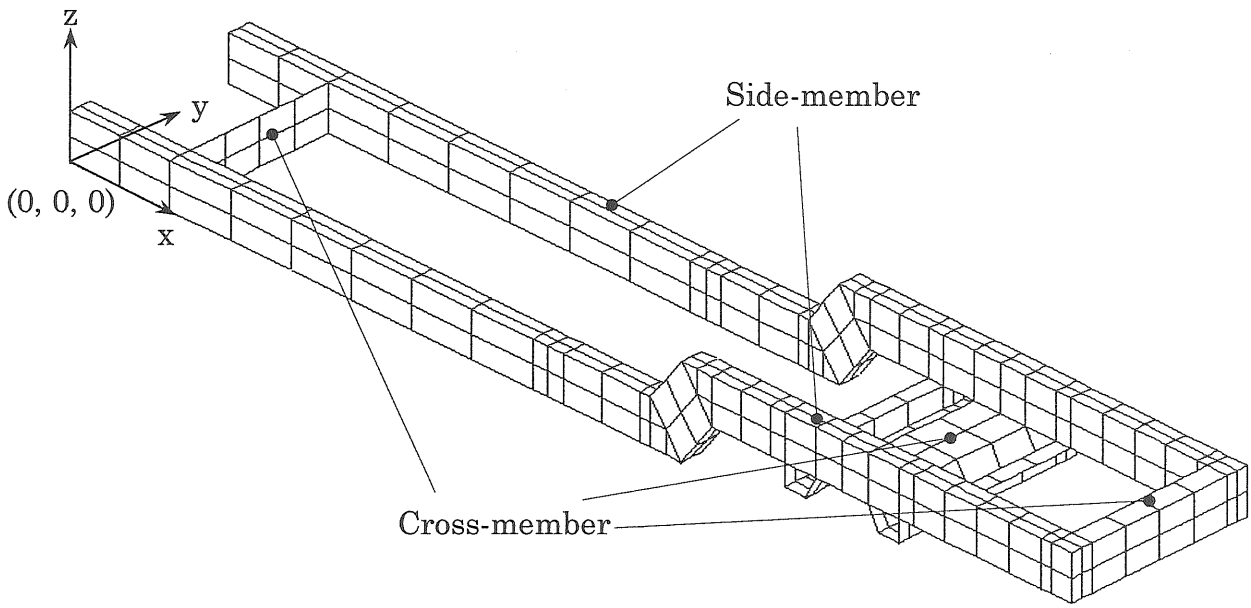

(b)

Fig. 4.1 Tractor frame: (a) frame allocation, and (b) its steel model.

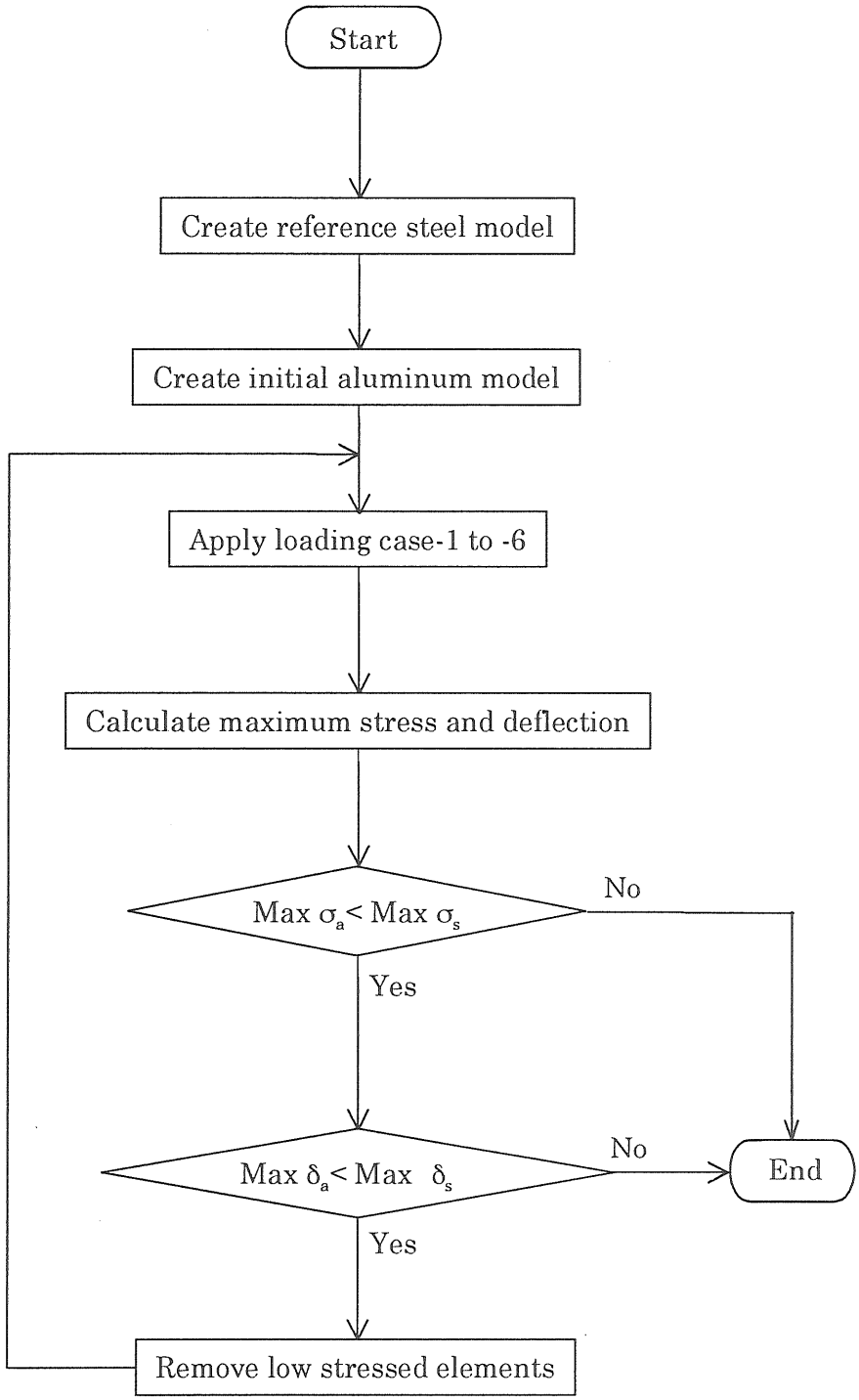

Notation:
σ_a: stress in aluminum model
σ_s: stress in steel model
δ_a: deflection in aluminum model
δ_s: deflection in steel model

Fig. 4.2 Development of FEM model for side-member.

member's height in the initial model was increased up to the maximum available space (Fig. 4.1).

After intensive calculation of mass, area moment of inertia and flexural stiffness on several type of beams, an I-type beam was picked since it has a comparatively higher ratio of moment of inertia to section area compared to other type of beams like rectangular-, U- and H-type beams. Despite its low stiffness in lateral direction, the I-type beam seemed to be adequate because most of the loads take place in the form of vertical forces. Moreover, a pair of side-members would be connected later with a number of cross-members that would boost lateral stiffness of the whole frame.

This study was intended to develop frame with minimum mass. Unfortunately, FEM5 program used in this study was not furnished with structural optimization module. Therefore, mass reduction effort was conducted manually. The outline of side-member model development process is given in Fig. 4.2. The process started with the creation of steel model for reference. Then, initial aluminum model was prepared using all available space (Fig. 4.1). While referring to the steel model for maximum stress and deflection under a set of predetermined loading cases, mass of the side-member was minimized by removing portions having lower level of stress. This process was repeated until "near minimum" mass was obtained.

This final side-member then served as the main member of the frame. Initial frame was assembled by connecting a pair of side member with several cross-member. The rest of the development process was similar to

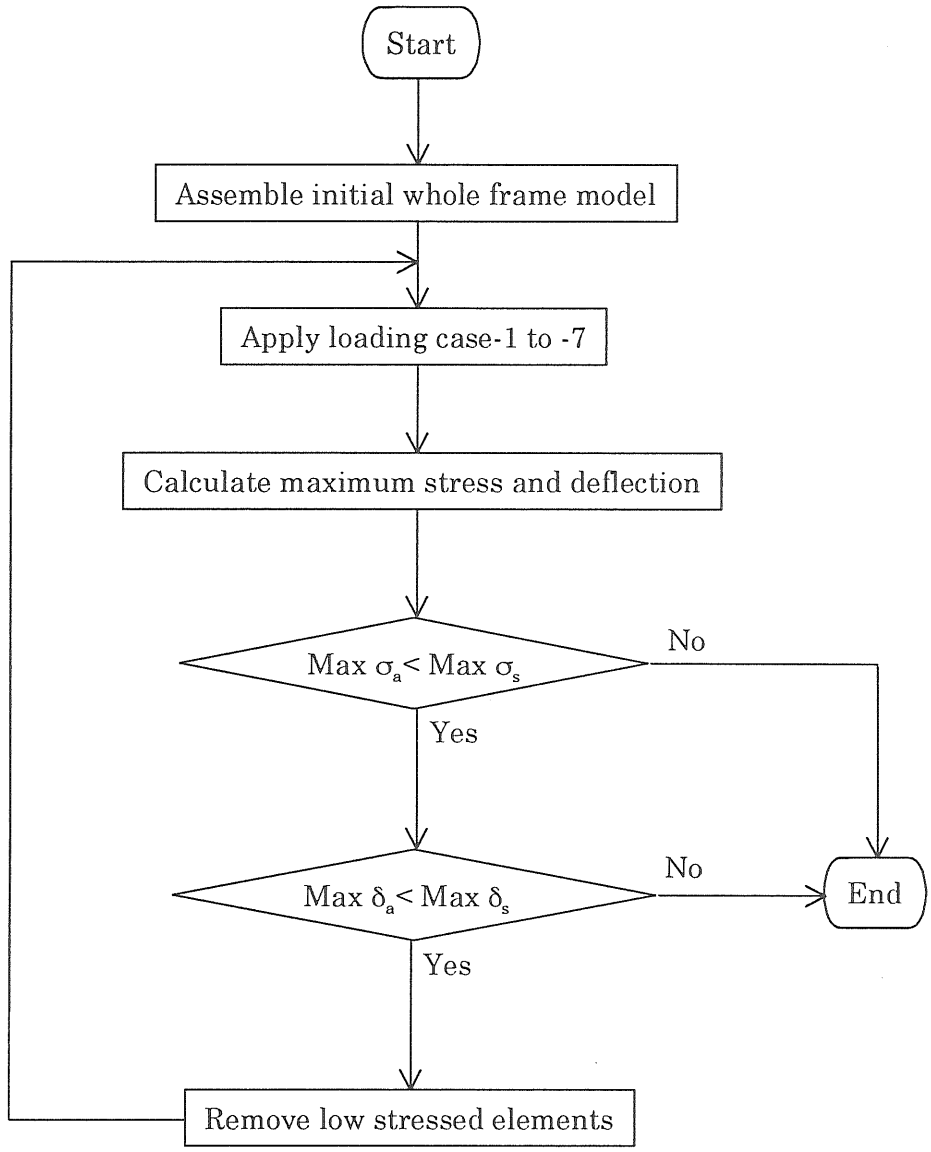

Notation:
σ_a: stress in aluminum model
σ_s: stress in steel model
δ_a: deflection in aluminum model
δ_s: deflection in steel model

Fig. 4.3 Development of FEM model for whole frame.

side-member model development (Fig 4.3). Regarding stress and deflection, steel model developed in Chapter 3 served as reference.

4.3.2 Applied loadings

Seven different loading cases were applied to the numerical models to simulate actual operating conditions. The first six loading cases followed exactly those introduced in the previous chapter, *i.e.,* body mass, front loader, front-mount earth-moving blade, mid-mount earth-moving blade or mower, and additional front mass. These were referred to as loading case-1 to -6. Loading case-7 described the external loads exerted on a tractor during turning operation at high speed. The forces considered in loading case-7 occurred at critical turning speed causing lateral overturn of a tractor.

The geometry of the tractor during turning is shown in Fig. 4.4. The relationship between critical turning speed, centrifugal force, and turning radius are described by the following equations[36]:

$$F_{cf} = m \frac{v_s^2}{r} \tag{4.1}$$

$$v_s = \sqrt{\frac{g\ C\ r}{z_{cg}\ \cos\ \gamma}} \tag{4.2}$$

where

v_s : critical speed, m/s

g : acceleration of gravity, m/s^2

C : horizontal distance between center of gravity and tipping line, m

r : turning radius, m

z_{cg}: height of the center of gravity, m

γ : angle between the assumed centrifugal force and the tipping plane, radian

F_{cf}: centrifugal force, N

m : mass, kg

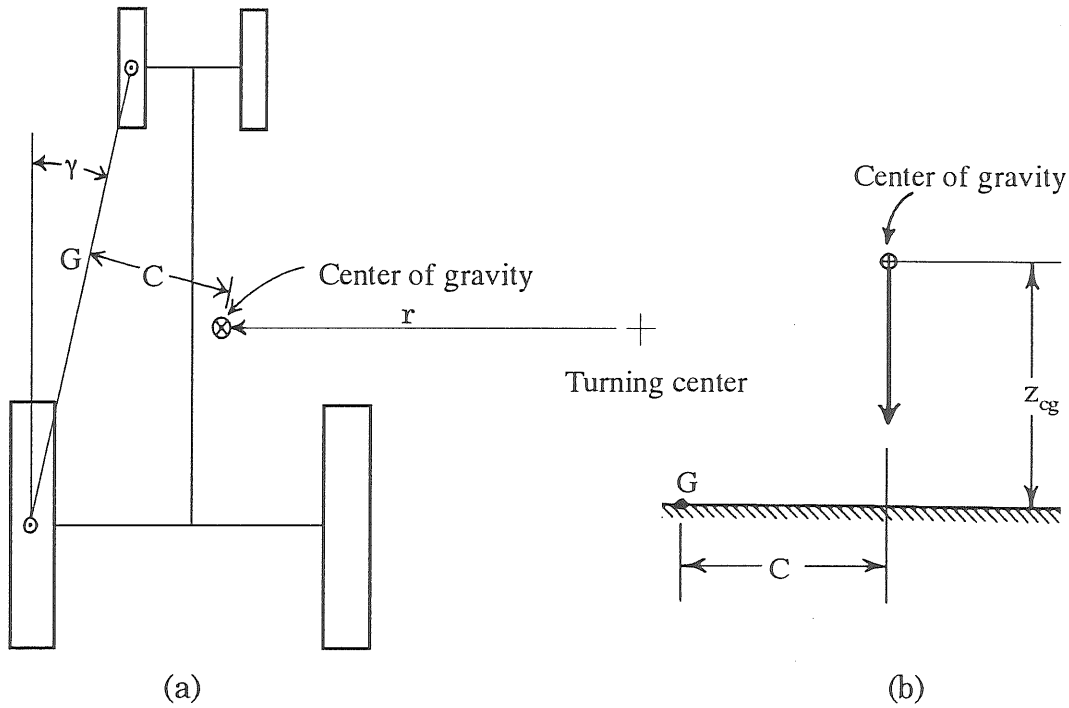

Fig. 4.4 Pertinent tractor geometry for lateral overturning analysis: (a) top view, and (b) plane view containing tipping motion of a tractor.

Measurements of tractor used in this study on flat ground revealed that C = 0.485 m and γ = 0.023 rad. Equation (4.1) indicates that critical speed depends on the turning radius. Furthermore, since C, z_{cg}, and γ are constant,

then υ_s^2/r becomes constant for a specific ground condition. According to equation (4.2), centrifugal force will also be constant. In this specific study, the tractor mass was 825 kg while the centrifugal force at critical speed with any turning radius was evaluated to be 6041 N.

The centrifugal force, which acts through the tractor's center of gravity,

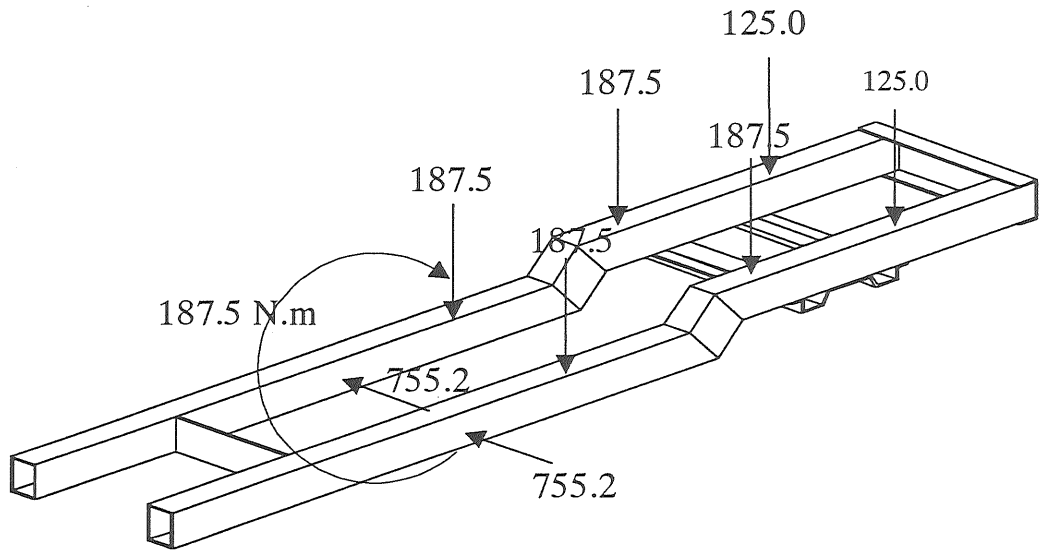

Fig. 4.5 Direction and magnitude of external forces in loading case-7. Digits denote forces in newton.

together with lateral reaction forces at the interface between the wheels and ground, creates a torsional force in the longitudinal direction of the frame to cause overturning. In addition, the centrifugal force and its lateral reaction forces on rear and front wheel also develop a lateral bending moment in the frame.

The schematic view of the direction and magnitude of the forces in

loading case-7 is shown in Fig. 4.5. The magnitude of all forces was scaled down with a force scale factor of 1:4.

4.2.3 Static and Eigenvalue analysis

(a) Static analysis

Just like the previous model, static strength of the models was evaluated. The analysis was the same to that in Chapter 3. Furthermore, for direct strength comparison between steel and aluminum model, it was more appropriate to use the strength-ratio instead of stress because steel and aluminum have different strengths. The following formula defines the strength-ratio[63]:

$$S = \sigma_y/\sigma_m \tag{4.3}$$

where

S : strength-ratio

σ_m: von Mises stress, MPa

σ_y : yield stress, MPa

For strength-ratio calculation, the yield stress was taken for evaluation of material failure instead of the ultimate strength because the former covers elastic behavior only. The value of the strength-ratio ranges from zero to infinity, and never becomes negative.

(b) Eigenvalue analysis

Eigenvalue analysis does not represent response due to any loading, but computes natural frequencies (eigenvalues) and corresponding mode shapes (eigenvectors) of the structure when there is no dissipation of energy due to damping. Natural frequencies and mode shapes are important in characterizing the behavior of a structure in response to dynamic loads and damping in modal dynamic analysis. Since in this study the analysis was only intended to find out the influence of structural modification on natural frequency, and the fact that modal analysis of tractor frame has been conducted by other researcher[25), 29)], modal analysis was not conducted.

The computation of natural frequency in FEM5 follows the process described in Fig. 3.4, but instead of solving the static equilibrium equation, it continues to solve the general eigenvalue problem below[*,67)]:

$$\{K\}\{\phi\} = \lambda\{M\}\{\phi\} \tag{4.4}$$

where

ϕ = eigenvector

λ = eigenvalue

Before computing the eigenvalues of the model, the validity of FEM5 module for eigenvalue analysis was verified by comparing results from numerical analysis to that from theoretical analysis for simple structures.

---

* Fujitsu Company. POPLAS®/FEM5 Manual for V25.

4.3 Results and discussion

4.3.1 Proposed FEM models

Figs. 4.6 and 4.7 presents the mass reduction process during the development of finite element models. As mass reduction progress, deciding which elements to be removed from the model became more difficult. This is reflected in both of the figures; the process progressed quite fast in the beginning, then became slower when it was close to the final shape. Total removed masses from initial shape were about 21.6% and 11.7% for side-member and whole frame model, respectively. This was, of course, far lower than that would be obtained by structural optimization programs. Motobayashi *et al.*[41] achieved mass reduction up to 45% using structural optimization program.

The final shape of the side-member for the aluminum model is shown in Fig. 4.8(a) while the whole frame model is shown in Fig. 4.8(b). The side-member model consisted of 769 nodes and 700 rectangular and triangular shell elements and with addition of cross-members elements, the whole frame model had 2101 nodes and 1968 elements. Compared with the steel model (Fig. 4.1), the depth of side-member of aluminum model was increased considerably. However, this would create difficulty in placing the engine on the frame. To correct this problem, the internal width of the rear portion of the model has been widened by 4 cm.

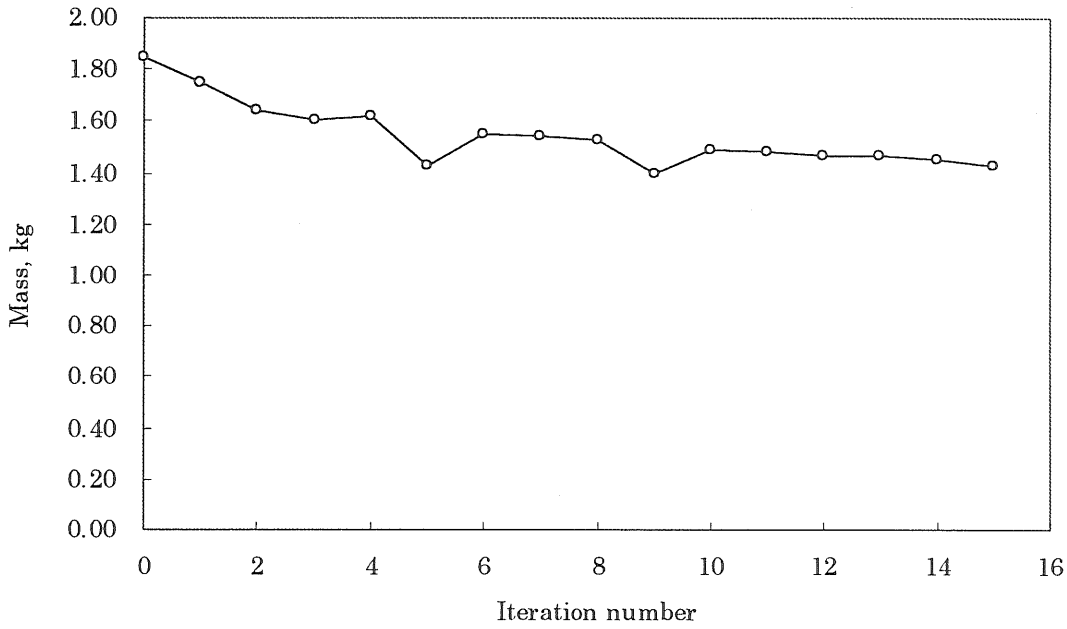

Fig. 4.6 Mass reduction process for side-member.

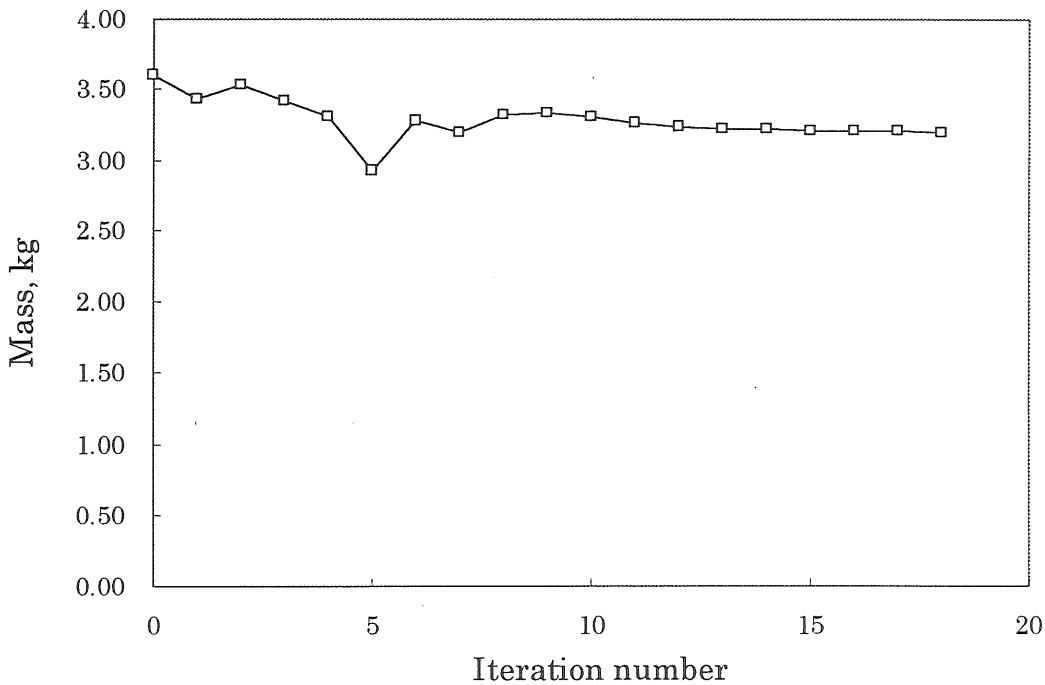

Fig. 4.7 Mass reduction process for the whole frame.

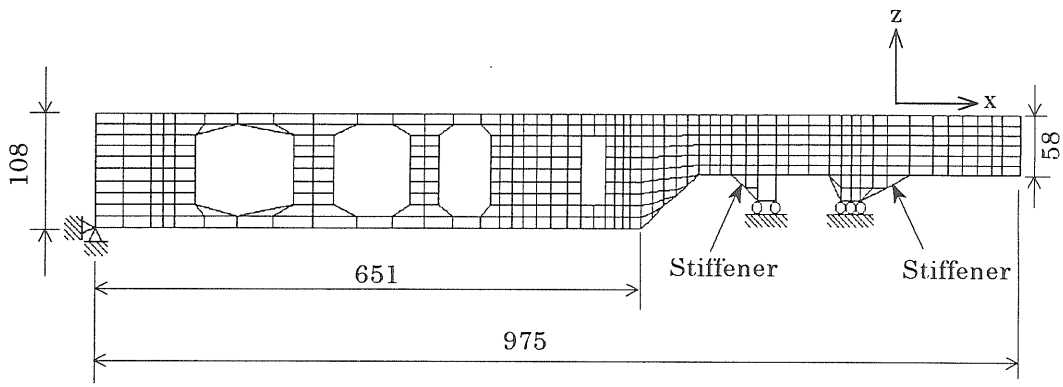

(a)

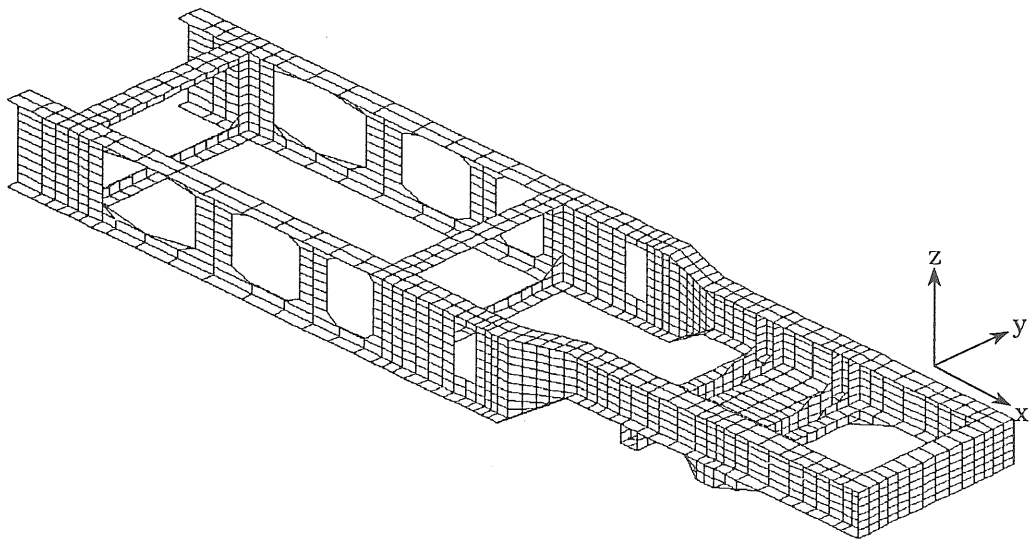

(b)

Fig. 4.8 Proposed aluminum model: (a) side-member, and (b) whole frame.

4.3.2 Structural strength and stiffness of side-member

The strength-ratio in six loading cases for both steel and aluminum models are presented in Fig. 4.9. As can be seen in the figure, their strength-ratio reached maximum values in loading case-1 and minimum value in loading case-2. The second highest strength-ratio also occurred in loading case-6. These values were inversely proportional to the magnitude of

forces in those loading cases. Loading case-1 showed the lowest magnitude of forces, while loading case-2 had the highest magnitude. While the total magnitude of the vertical forces in loading case-1 was 1000 N, the total magnitude of vertical and horizontal forces in loading case-2 were 8315 N and 4280 N, respectively.

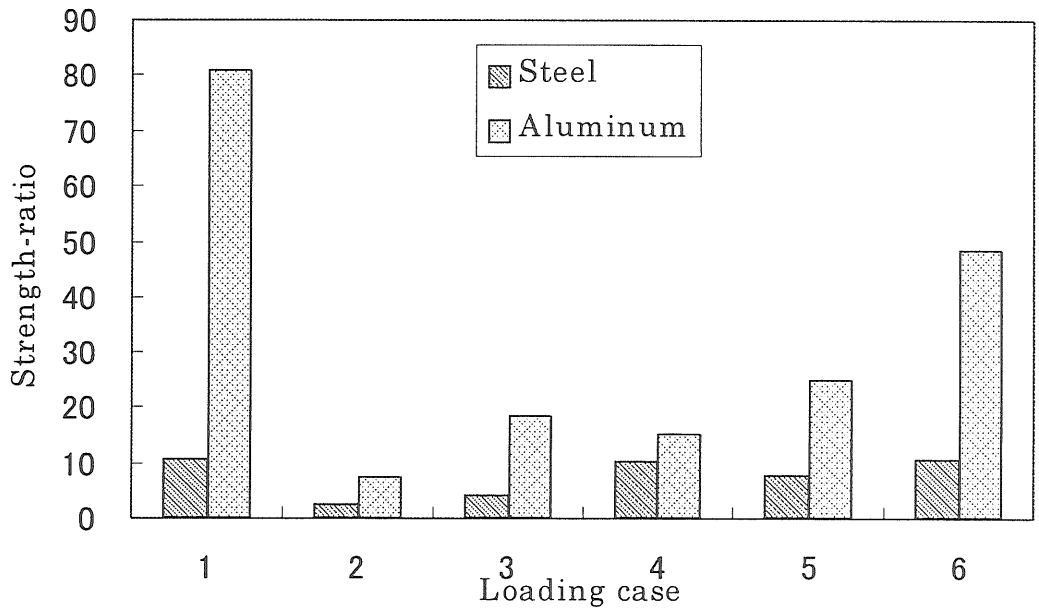

Fig. 4.9 Strength-ratio of side-member under loading case-1 to 6.

Despite these results, both steel and aluminum models indicated slightly different patterns in relation to the strength-ratio. For example, the second highest strength-ratio for the steel model occurred in loading case-3, while that of the aluminum model occurred in loading case-6. Other distinct features exist in the maximum and minimum value of strength-ratio. While steel model reached its maximum value of 11 in loading case-1, the aluminum model had its maximum value of 81. Furthermore, the minimum

value of the strength-ratio of the steel model was 2.3, whereas the corresponding value of the aluminum model was 7.5. Considering that the minimum strength-ratios of steel and aluminum were 2.3 and 7.5 respectively, it is evident that the aluminum model is capable of supporting higher loads than the steel model.

The strength-ratio is closely related to safety factor, which has been widely used to assess the safety or strength of a structure under a particular loading. Again, by comparing the minimum value of the strength-ratio for the steel and aluminum models, which were 2.3 and 7.5 respectively, with the safety factor of 3 typically used in machine-design applications[61], it can be indicated that safety factor for steel was lower compared to aluminum in this case. Accordingly, for the loading combinations involved in this analysis, the aluminum model was confirmed to be safer than the steel model.

Examination of the strength-ratio showed that the most critical loading was loading case-2. To understand further the strength characteristics of the models in this specific loading, further discussion regarding stress distribution is necessary.

Fig. 4.10 describes the von Mises stress distribution under loading case-2 in the steel and aluminum models. In the steel model, maximum stress occurred at node no. 208 with 98.7 MPa, which is directly above the end-portion of cross-member connection to the side-member. In this node, the bending stress due to applied forces in the front portion of the frame reached its maximum value.

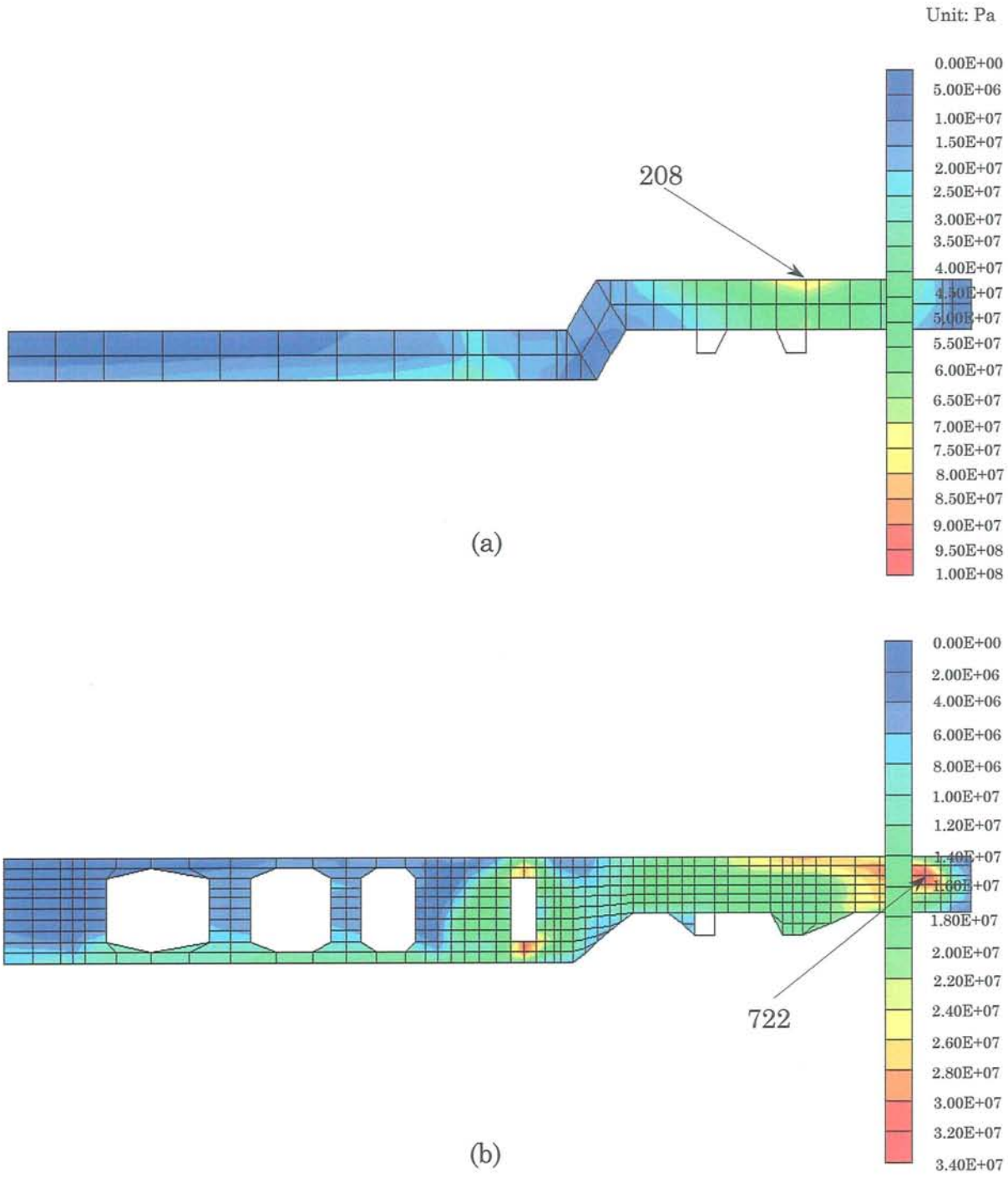

Fig. 4.10 Stress distribution under loading case-2: (a) steel, and (b) aluminum. Digits denote node number.

Prior to attachment of stiffeners (Fig. 4.8), similar stress patterns also occurred in the aluminum model. After the addition of stiffeners, the locations at which highest stress took place shifted forward beyond the

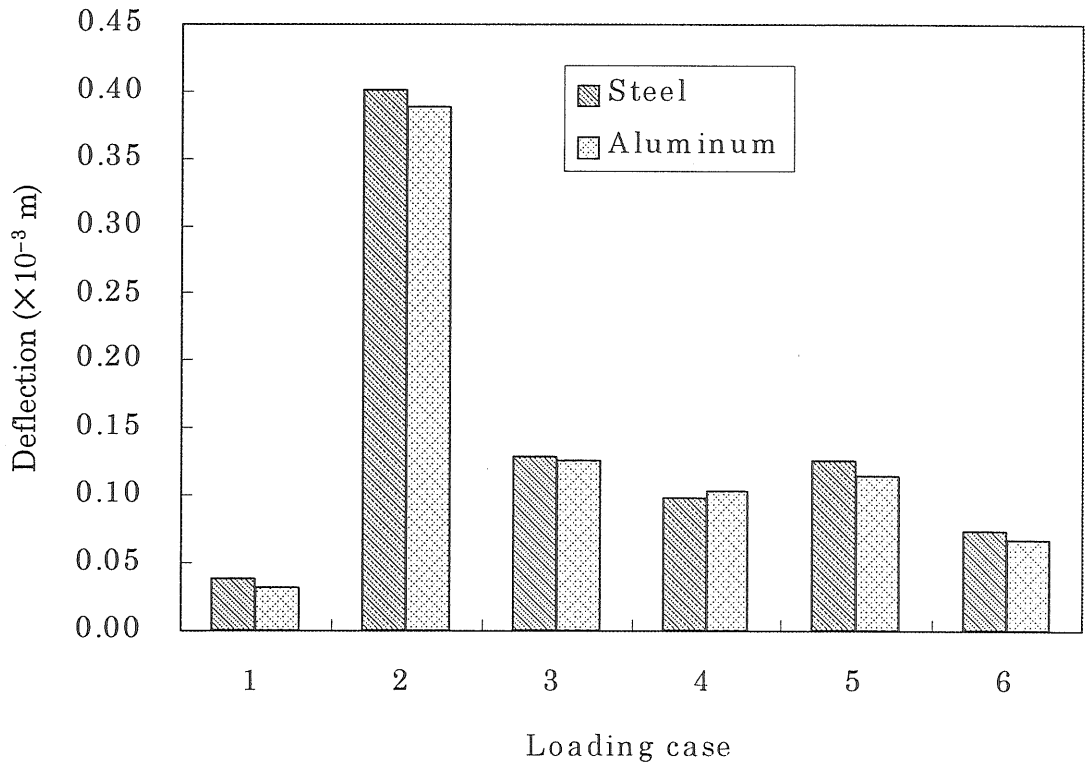

Fig. 4.11 Resultant deflection of the side-member under loading case-1 to 6.

cross-member connection up to node number 722. The von Mises stress in this node was 45.7 MPa, or about 50% of the corresponding value in the steel model. This significant decrease of maximum von Mises stress when steel was changed to aluminum was due to increase in sectional modulus of aluminum members. At this portion, the sectional modulus increased by 3.3 times.

In elastic range, the resultants of x-, y-, and z-deflection under different loading cases are given in Fig. 4.11. It shows that, like the aluminum model, the steel model reached its maximum combined deflection in loading case-2, whereas its minimum combined deflection occurred in loading case-1. This directly coincides with the maximum von Mises stress for loading case-2 (Fig. 4.9).

Figure 4.11 shows that, not only was the trend in combined deflection similar, but the magnitude of deflections were also very close. Except in loading case-4, the deflection on aluminum was always slightly lower than that of steel. This decrease in deflection was due to an increase in flexural rigidity. Although aluminum's modulus of elasticity was only 1/3 smaller than steel, the aluminum member had a ten times bigger moment of inertia, and its flexural rigidity became 3.5 times more than the steel.

The deflection in z-direction of the proposed model was always smaller than that of steel model. Nevertheless, in x-direction, deflection in the aluminum model was higher by about 6%. Realizing that most, and the strongest dynamic load acts in z-direction[48), 49), 54)], this drawback will not significantly affect the tractor stability during its operation.

The higher deflection in x-direction was due to low stiffness of aluminum. Although its cross-sectional area, A, has been increased by 1.9 times, its value of $A \times E$ was still lower compared with that of steel. To increase $A \times E$, an increase in cross-sectional area is recommended, although this approach may not be realistic because of increase in mass.

It can be observed that the two models were similar in strength and deflection patterns under loading case-1 to -6. Just like the aluminum model, the steel model exhibited its lowest strength in loading case-2. Besides this specific trend, both models showed substantial differences. Eventually, the aluminum model exhibited about three times higher strength than the steel model.

4.3.3 Comparison of aluminum model with an optimized steel model

Earlier research in our laboratory concerning mass reduction on this type of frame was conducted by Motobayashi et al[41]. They used the shape optimization module SHAPE of NISA family to minimize the volume of a side-member model while maintaining equivalent strength characteristics.

The software offered two modes of optimization: general optimization mode and boundary optimization mode*. In the process of volume minimization, the general optimization mode allowed material removal from anywhere in the structure except for regions frozen by the designer. Using this optimization mode, material removal might result in holes and cavities within the structure, thus creating a new shape, which is useful in proposing a basic shape for a new styling. In contrast, the boundary optimization mode allowed material removal only at the vicinity of the existing boundary, thus without creating new boundaries. This mode of optimization was appropriate

* EMRC. 1989. SHAPE user's manual. Enginering Mechanics Research Corporation, Troy, Michigan.

to be used when the basic shape of the system is known or when many of the regions have already been frozen by the designer.

Motobayashi *et al.* used the two mode of optimizations to the initial shape as shown in Fig. 4.12(a). This model was composed of 2956 triangular elements and 1614 nodes enabling two degree-of-freedoms each. The two optimization modes produced different results. While the general optimization mode produced a model with 26% mass reduction (Figs. 4.12(b) and 4.12(c)), the boundary optimization mode finalized with a mass reduction of 42%. Despite these advantages, the boundary optimized model includes considerably higher stress and deflection compared with the original model. This optimized model has a considerably lower mass, about 30% less than an aluminum model. Despite such an advantage, as illustrated in Figs. 4.13 and 4.14, the strength performance of this model was lower than the aluminum model under any loading case. Even in some cases, its strengths were clearly too low. For example, maximum stress under loading case-2 of 1107 MPa was bound to be beyond the yield stress. The main reason for this drawback was that the shape optimization effort based only on loading case-1, which actually generated the lowest stress level compared with other loading cases. In contrast, mass reduction effort in for aluminum model in this study was based on loading case-1 to 6. Although the mass reduction was not very high, it met all the basic requirements.

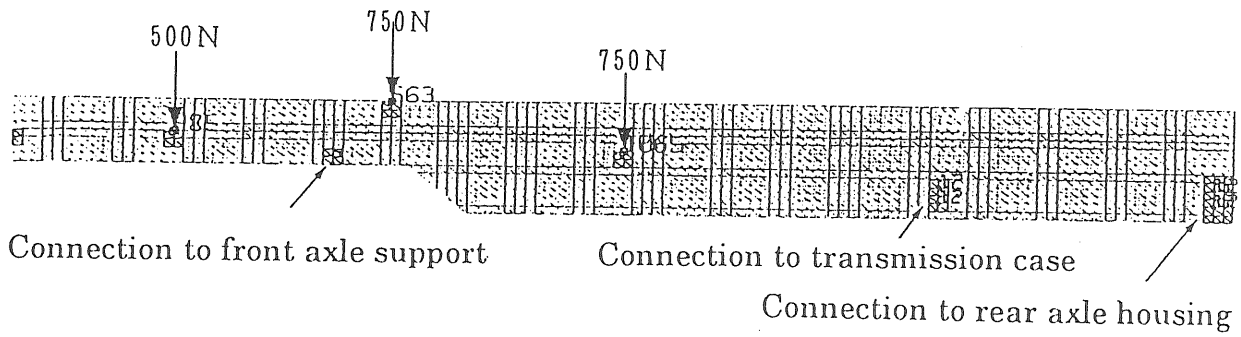

(a) Initial shape

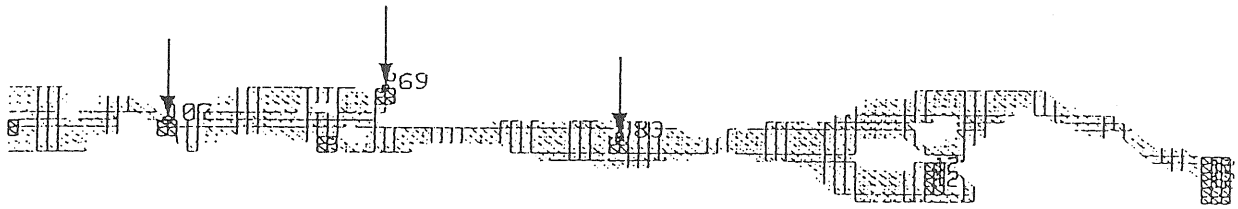

(b) Optimum shape

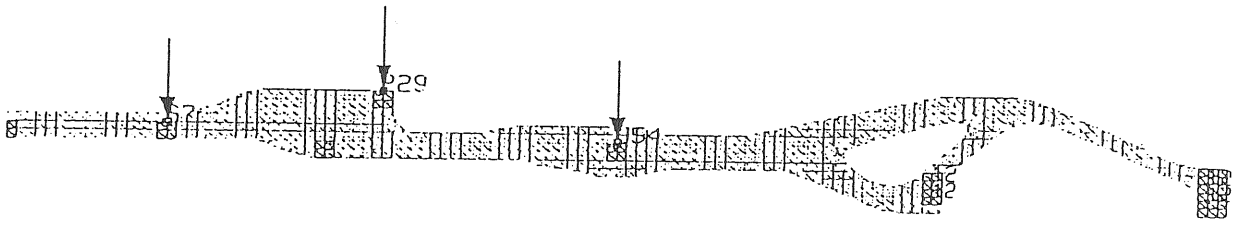

(c) Boundary smoothed shape

Fig. 4.12 Model of optimum shape analysis (after Motobayashi *et al.*[51]).

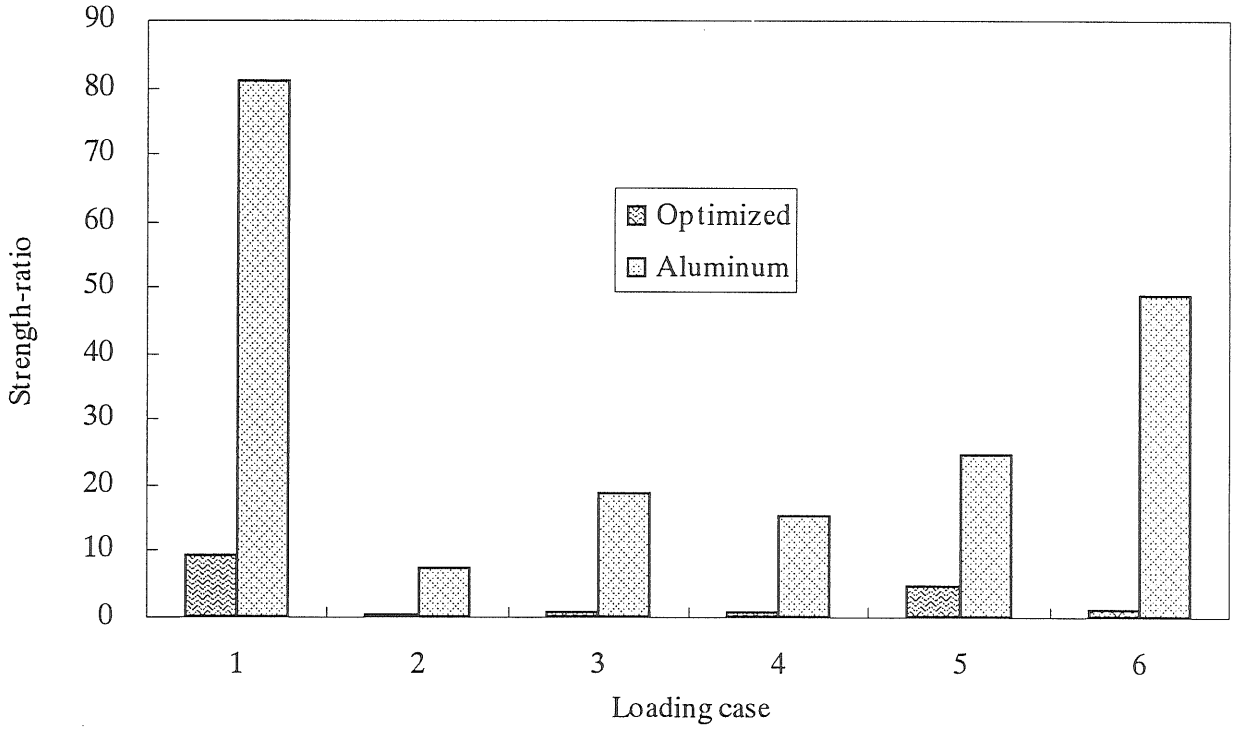

Fig. 4.13 Strength-ratio of aluminum and optimized steel model.

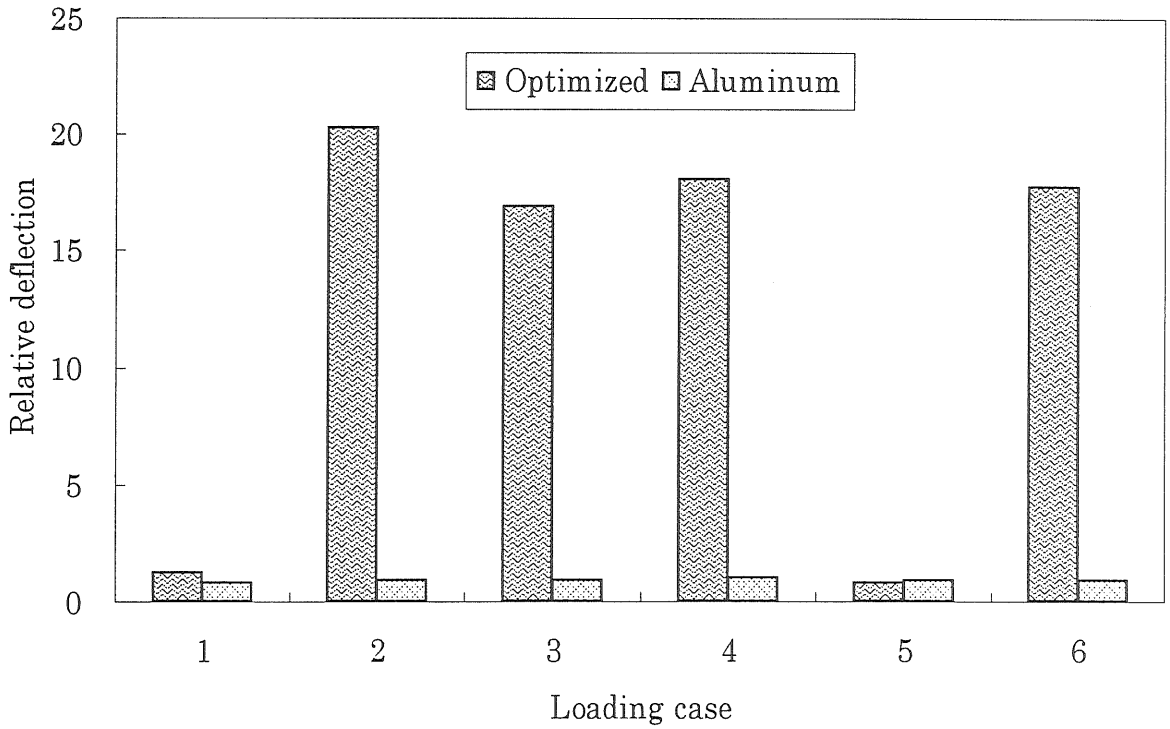

Fig. 4.14 Relative deflection of aluminum and optimized steel model.

4.3.4 Structural strength and stiffness of the whole frame

The loading case-1 to 6 were used again to examine the whole frame behavior under static loading as shown in Fig. 4.15. Similar trends in the strength-ratio of the side-member for the steel and the aluminum model were observed. However, the values of the strength-ratio were somewhat lower than the values of side-members. For example, the strength-ratio for the aluminum frame in loading case-1 became 59 while the side-member had 81. This difference was due to change in the location of supporting points in front portion of the frame. In side-member analysis, the locations of the supporting points were fixed at the bottom of the side-member (Fig. 4.8). In this analysis, the supporting points were moved to the middle of the cross-member above the front axle. Consequently, the cross-member had to support forces that were about twice the magnitude of those in side-member analysis.

Figure 4.15 also shows that the lowest strength-ratio for steel and aluminum model was developed in loading case-7. The minimum values in terms of the strength-ratio were 2 and 3 for the steel and aluminum models, respectively. Therefore, it can be deduced that the strength of the aluminum model was higher than that of steel model.

Loading case-7, which represented turning at critical speed, produced the highest level of stress among all applied loadings. In addition to higher forces, loading case-7 incorporated forces that caused lateral bending and torsional loading. The stress distribution within the frame due to this load is

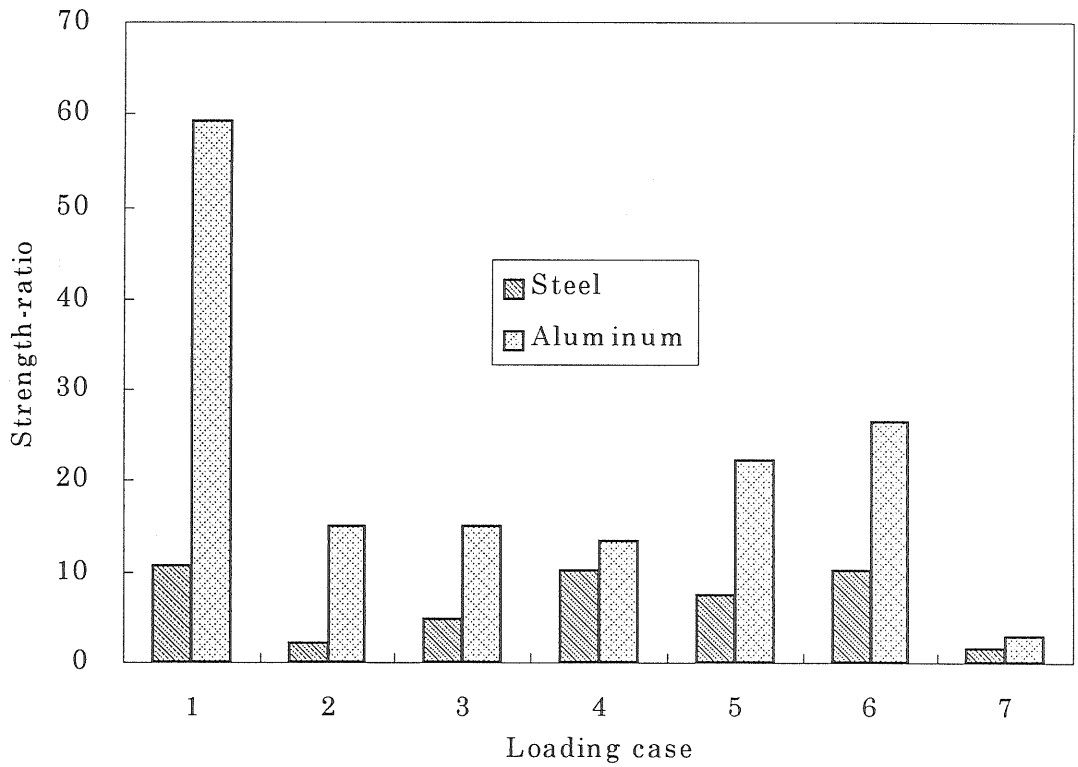

Fig. 4.15 Strength-ratio of the whole frame under loading case-1 to 7.

revealed in Fig. 4.16. In the two models, the highest stress level could be found in side-member on farthest side from the turning center. Substantially higher stress occurred in the steel model compared to the aluminum one. For the steel model, the maximum stress occurred at node no. 75 indicating 147 MPa, while for the aluminum model it was node no. 324, which reached 103 MPa. The aluminum model incurred lower stress level than the steel model because of an additional cross-member in the middle part of the aluminum frame. The presence of this cross-member reduced bending stress in lateral direction by reducing the length of moment arm and transmitting some loads to other side-members. Moreover, the higher number of cross-members also

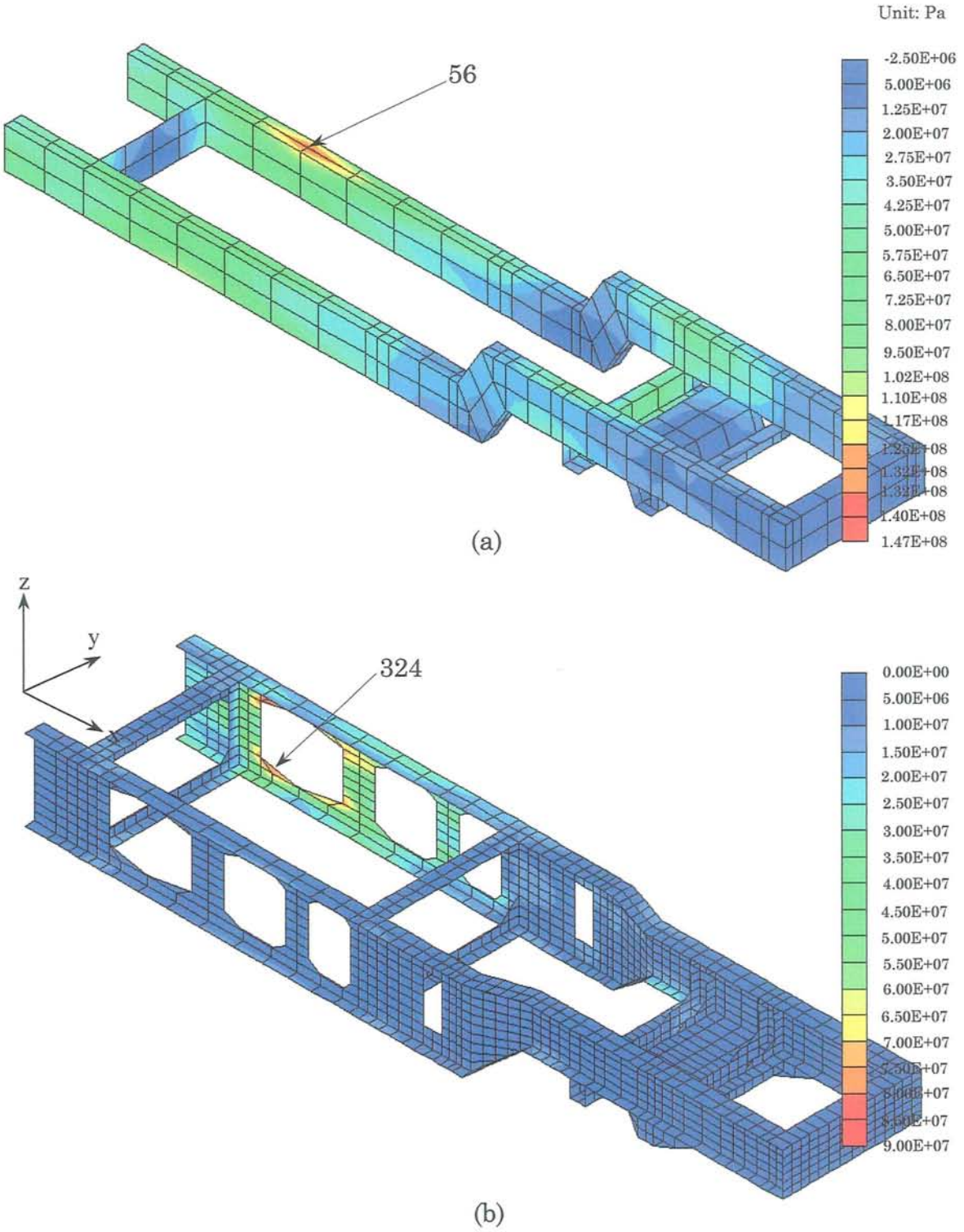

Fig. 4.16 Stress distribution under loading case-7: (a) steel, and (b) aluminum. Digits denote node number.

decreased stress level generated by torsional loading as they provided a larger area for the same level of applied load.

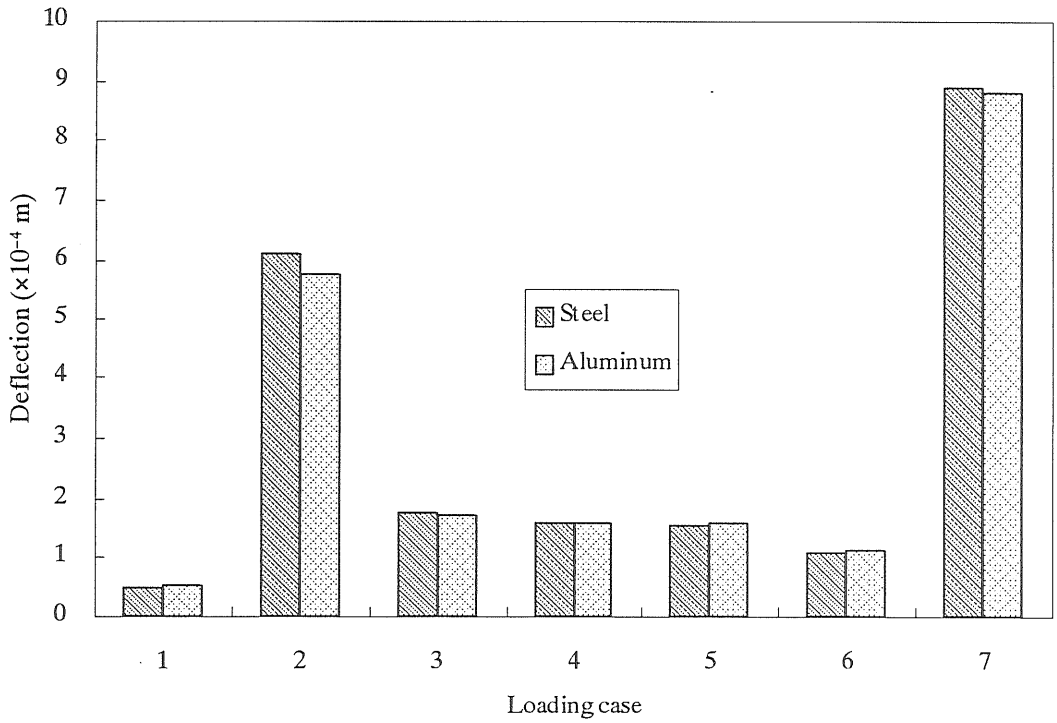

Fig. 4.17 Resultant deflection of the whole frame under loading case-1 to 7.

Figure 11 describes the computational results concerning combined deflection for both models. Although the deflection on the side-member of the aluminum model was lower compared with the steel model (except for loading case-4 in Fig. 4.11), the maximum deflection of the whole model exhibited different strength characteristics. As can be seen in Fig. 4.17, the stiffness of the aluminum model was slightly lower in loading case-3, -4, and -6. In these loading cases, the deflection of aluminum model was about 2-4% higher than that of steel model due to low flexural stiffness of cross-member

above front axle. Actually, this portion has been modified considerably by utilizing all available space; nevertheless, its flexural stiffness was still lower than that of steel. Due to space restriction, it seems difficult to increase stiffness of this part without increasing its mass. Naturally, by using material with higher stiffness, this problem may be solved.

4.3.5 Attained mass reduction and possible benefit

In the process of developing the aluminum side-member, a minimum mass of 1.452 kg for a single member was achieved. Compared with the corresponding steel member, which showed a mass of 2.195 kg, mass reduction reached 34%.

After mass minimization of the whole frame, the total mass of the aluminum frame became 3.198 kg while the steel had 4.423 kg (28% mass reduction). This is a favorable indication particularly when compared with the previous aluminum model, which only attained 20% mass reduction.

The fact that the mass reduction of the whole frame was lower compared with that of the side-member signified that partial mass reduction in cross-members was less compared with that of side-members, especially for the front cross-member. Actually, most of the elements in the middle portion of the front cross-member have significantly low stress level such that their removal would not be related to the frame's strength as well as the frame's torsional stiffness. Nevertheless, due to its function for attaching ballast and front hitch implement they were retained.

One portion in which mass reduction was not significant was cross-member above the front axle, although its shape has been thoroughly modified. The main reason is that this component is located in a quite restricted space, especially its depth. As stated in Section 4.3, gain in mass reduction for a stiffness-based design will be maximized by increasing depth of beam. Such approach could not be practiced here, since the component is located in a restricted space. Considerable mass reduction may only be achieved by redesigning the cross-member connection to the front axle and the connection of engine to the frame in which extra space should be provided for escalation in the depth of the cross-member.

Mass of a tractor frame is only a small fraction of the whole tractor mass. Although frame mass has been reduced by 28%, in terms of total tractor mass, mass reduction was only roughly 2%. Nevertheless, if this approach of mass reduction is also applied to other portions of the tractor such as the transmission case, clutch housing and engine block, a major decrease in mass could be expected. Miki[39] predicted that mass reduction in major portions of the tractor excluding the frame would result in the decrease of mass up to 28%. Thus, total mass reduction by using aluminum could become 30%.

Many of the dynamic forces working to tractor structure during actual working condition are proportionally related to the tractor mass such as centrifugal force during turning, impact force when tractor pass a bump or a ridge. Thus, if the tractor mass can be reduced considerably, these forces will

alleviate markedly. Consequently, tractor components can be constructed significantly smaller and lighter.

With substantially lower mass, energy consumption of tractor may be lower. Due to the nature of task assigned to tractor, gain in fuel efficiency due to mass reduction will not as high as that of a car. Car is used to transport its payload while tractor is mainly used for towing implement. When tractor is not used for towing implement, such as when commuting between field and farmer house, spraying and rotary tilling, the gain in fuel efficiency is the same as that in car. Nevertheless, when tractor pulls heavy implement such as in plowing and transporting harvested materials, a large amount of ballast is added to generate enough traction at drive wheels, therefore, no gain at all in terms of fuel efficiency. In case tractor pulls low-draft implements such as harrows and cultivators, the quantity of gain in fuel efficiency depends on the amount of ballast added to tractor to produce required traction at drive wheels. It is when pulling this various type of implement, lightweight tractor provides wider room for ballast optimization. Moreover since traction efficiency of lightweight tractor attains its maximum value at lower slip, maximum power can be achieved only at high speed.

Traditionally ballast for agricultural tractor are in the form of liquid in drive wheel or cast iron at the side of drive wheels and in the front of tractor. These ballasts are static in nature, that is, the force they exert on the tractor wheel are constant throughout tractor operation. Ideally, owing to the fact that draft varies throughout operations, this force should adjust accordingly.

In line with this idea, recently, there have been proposals to design dynamic ballast system by which the weight distribution on tractor wheels can be optimized according to draft created by the pulled implement[9),66)]. Experiment showed that this type of ballast system could save fuel consumption of a standard tractor by about 5 to 15%. For a lightweight tractor, which provides wider room for ballast optimization, it is believed that gain in fuel efficiency will be much higher.

The other way of capitalizing this light mass tractor is by simultaneously attaching implements in the rear and front of the tractor. Rear attached implement, which is commonly used with standard tractor, transfer weights from front wheel to the rear ones and tends to lift front wheel. Therefore, to avoid rearward overturning, ballast should be added in the front of the tractor. Contrary to rear attached implements, front attached implement tend pull the front wheel down and lift the rear wheel up[13), 28, 62)]. If both of rear and front implements are used, and they are arranged in proper combination, ballast may no longer necessary to increase traction. Thus, energy to carry the ballast can be saved. Although currently most of the implements are rear attached ones, many of the latest standard tractors are equipped with front hitch attachments and it seems that front attached implements will be more popular in not too distant future[50)].

Other promising area of application is in paddy-field operation. In many Asian countries, rice is mostly grown in paddy-field. During tillage and planting time, due to flooded condition, soil became very soft and has very

low bearing capacity. In this condition, most tractors use cage wheel instead of rubber wheel. Cage wheel offers better traction and flotation in most condition. For field with lower bearing capacity, special flotation device is necessary[27), 51), 55)]. Because of this mobility problem, most of power transfers in wetland operation do not use drive wheel, but PTO (power take-off) such as rotary tiller. Thus, weight at drive wheel may be maintained at minimum just for moving the vehicle. Based on this consideration, lightweight tractor is more suitable for wetland operation. With lightweight tractor, flotation device may be built smaller and lighter.

4.3.6 The effect of structural modification on natural frequency

(a) Program verification

Seven simple structures have been selected as sample problems for verifying the eigenvalue analysis module of FEM5. The structure ranges from simply supported beam to free edged square plate, and each composed of bar-, shell-, or solid-type elements. Simple structures were chosen instead of more complicated ones because their theoretical solutions are readily available in standard textbooks[11), 57), 60)].

The result summary of eigenvalue analysis of the sample problems and their corresponding theoretical solution are given in Appendix D. Table 4.1 presents the summary of comparison between the theoretical and numerical results. Number of modes is not the same for all the problems, but depends on the available theoretical solution. As can be seen in the table, the errors

Table 4.1 Difference (%) between theoretical and finite element solution on selected eigenvalue problems

Mode	Problem number*						
	1	2	3	4	5	6	7
1	3.0	0.6	1.5	0.5	0.6	1.3	0.1
2	2.8	1.9	2.2	1.2	0.8	1.4	2.7
3	2.9	1.9	5.3	0.2	0.9	2.2	2.9
4	8.8	2.0					1.4
5	4.6	3.5					3.8
6							3.8
7							5.6

*

1 Square cantilever plate, shell element
2 Simply supported square plate, shell element
3 Free edged square plate, shell element
4 Cantilever beam, bar element
5 Simply supported beam, bar element
6 Unconstrained beam, bar element
7 Cantilever beam, solid element

range from 1 to 6%. These are quite small; therefore, it can be concluded that results from FEM5 are in good agreement with the theoretical ones.

(b) Computation results

The dynamic behavior of any structure depends on its natural frequency. If natural frequency of a member or the whole structure coincides with excitation frequency, resonance will occur. In this condition, even very small excitation will develop into high-amplitude vibration, which can be disastrous not only to the operator but also to the structure itself. Furthermore, a similar situation will occur if the natural frequency of a member overlaps with other member's natural frequency. Without proper damping, vibration in one member will induce vibration in others. Like other machines, the natural frequency of a tractor's component has to be within a certain range so that tractor can perform well.

Basic equation for natural frequency of any structure having mass m and spring constant k is given by equation (4.5). With this equation, we may roughly predict the change of natural frequency due to structural changes in tractor frame. In this study, the proposed aluminum model had nearly the same stiffness but at substantially lower mass. Therefore, we may expect that its natural frequency will be higher than that of steel.

$$f = \frac{1}{2\pi}\sqrt{\frac{m}{k}} \tag{4.5}$$

Table 4.2 presents the computation results on natural frequency for the first five modes. In accordance with prediction, natural frequencies aluminum in the first and the fifth modes were 15% higher than that of the steel model and were only 4% higher in the fourth mode. In the second and third modes, however, they were 3 and 5% lower than the steel ones. These seem opposite results was due to the fact that the change of mass and the level of stiffness was not the same for all frame components. For example, in the cross-member above the front axle, a slight decrease in mass also followed by a substantial decrease in stiffness. In turn, it may cause a decrease in natural frequency at certain modes. This is similar to a research by Clijmans *et al*[10]. They reported that additional 50-kg ballast placed in front of the tractor did not change most of the natural frequency except its fourth mode that decreased from 4.27 to 4.17 Hz. However, when an additional metal truss was fixed between two locations in its cab, its natural

frequencies in the fifth and sixth modes shifted beyond the frequency band of the study.

Table 4.2 Natural frequency (Hz) of steel and aluminum model

Mode no.	Steel	Aluminum
1	40.3	46.4
2	266.6	258.6
3	331.8	315.7
4	365.0	378.6
5	387.1	446.2

During normal operation tractor undergoes various excitation. Vertical excitations from terrain are in the range of 1 – 10 Hz[5), 35)]. The longitudinal and lateral motions of chassis and cab are from 2 – 12.4 Hz[38), 54)]. The natural frequency of tractor itself usually is in the range of 2 – 4 Hz[5)]. In general, it may be stated that the excitations to tractor are in the range of 1 – 20 Hz. These frequencies are far below the natural frequencies of the proposed chassis. Therefore, it may be predicted that during normal operation, chassis will not be subjected to resonance.

4.4 Summary

A new aluminum model has been proposed to improve mass reduction and stiffness of the first model. Mass minimization was applied manually and succeeded to decrease overall frame mass by 28%. In all loading cases

employed in this study, the aluminum model exhibited higher strength compared with the existing steel model. Depending on the working load, aluminum frame was 1.5 to 6 times stronger than that of steel. Furthermore, the stiffness of side-members in the aluminum model was higher compared with that of the steel one; however, its cross-member stiffness was slightly lower. In general, the stiffness of the whole frame model was nearly the same.

Several simple structures have been chosen to verify the eigenvalue analysis module of FEM5. Results showed that there was a good agreement between numerical and theoretical solutions. Moreover, computation on frame models revealed that natural frequencies of the aluminum model were not much different from that of the steel one. These natural frequencies were far above excitation frequencies from the ground and the natural frequency of the tractor.

Chapter 5
Conclusions and recommendations

In this research work about the structural characteristics of aluminum-made chassis-type frame of a tractor, efforts on mass reduction of a chassis-type frame of a tractor using aluminum were conducted. In the first approach, aluminum was used to substitute steel in the original tractor's frame design. For this purpose, two numerical models for steel and aluminum were developed and their structural characteristics were evaluated numerically using FEM. Loading tests were then carried-out to verify the results from numerical analysis. To improve the structural characteristics of the first aluminum model, then the shape and size of the main members of the model were modified and their mass were minimized. Finally, to investigate the effect of this structural modification on natural frequencies of the frame, eigenvalue analysis was performed.

5.1 Conclusions

Based on the research work, the following conclusions can be drawn:

1) Aluminum can be effectively used for mass reduction of a steel structure, even without modifying its basic design. For a strength-based design, the effect of mass reduction is attainable up to 50%, while for a stiffness-based design it is far less than this figure.
2) Mass reduction using aluminum can be effective only if sufficient extra space is available around the original structure. This space is necessary

to allow an increase in size of the structure to compensate the lower modulus of elasticity and strength of aluminum. For strength and stiffness based design, substantial mass reduction cannot be achieved in a restricted space.

3) The first aluminum model, which was basically the same with the original steel model in configuration and member's shape but had one additional cross-member, achieved a mass reduction of 20%, at nearly 2 times strength but 13% less vertical rigidity. Results from subsequent loading test confirmed this FEM results. This also served as a verification of the FEM5 program used in this study

4) The second aluminum model, which was developed by modifying the shape and size of cross- and side-member, achieved a mass reduction of 28%. In terms of strength, this model was 1.5 to 6 times stronger than the steel one. Moreover, contrary to the first model, this level of strength has been achieved with nearly the same level of stiffness.

5) Results of FEM showed that structural modification on frame did not much affect its natural frequency in the first five modes. Only natural frequency of the fifth modes increased substantially by this modification. It increased by 15%.

5.2 Recommendations

This research has shown methods of mass reduction of a steel structure with aluminum. These methods can also applied to other agricultural

machinery. However, before applying these methods to other machinery or putting this design into production line, some refinements and further analysis are necessary. For this, the followings are recommended:

1) Computations and tests in this research were conducted on model with a scale of 1:2. Because, usually there is scale effect, working model with actual size will likely produce more accurate results.
2) This research only deals with static analysis. Actually, as tractor works in fields, the forces exerted on tractor structure changes dynamically with time. Therefore, dynamic analyses such as modal analysis, frequency spectrum analysis are necessary.
3) Fatigue is one of the pertinent problems of aluminum structure to be clarified. This research will be useful if a discussion regarding fatigue analysis to be added.
2) Effort to reduce tractor's mass should be continued to other heavy components such as engine block and transmission case. In these components, substantial mass reduction will undoubtedly be attained by introducing aluminum. Mass reduction effort on these two components will likely more difficult because load will not just external force like in chassis but also heat generated by engines and rotating parts.
3) This method of mass reduction may be applied to other agricultural field machinery such as harvester. Due to the nature of harvester operation in the field, in any condition harvester will not need any ballast to perform properly. This will make mass reduction more rewarding effort.

4) Before a design is put into production line, a financial or economic analysis is usually a mandatory. In case of aluminum chassis for tractor, it should not confine itself to manufacturing aspect, but also include frame's whole service life. Although at present manufacturing condition an aluminum chassis is still more expensive than the one of steel, if outfitted with proper ballast, a considerably lighter tractor will certainly consume less energy and produce less soil compaction during its service life.

Acknowledgement

The author's greatest debt is to Prof. Masayuki Koike, his thesis adviser, who continuously gave guidance and advice during the whole research and study periods. His endless suggestions, and helps in all aspects of this research are very much appreciated.

The author also expresses his deep sense of gratitude to his examination committee members: Associate Professor Tomohiro Takigawa, who gave guidance for making electronic circuit to measure displacement on experimental models and later lending his own laser displacement sensor for more accurate measurements, Prof. Masayoshi Sato and Prof. Naoki Sakai, who gave their invaluable suggestions and corrections to improve this thesis.

He also feel very indebted especially to Dr. Hideo Hasegawa for giving advice and many useful ideas when the author stumbled into computational problems, Mr. Akira Yoda for correcting drawing and procurring the material for experimental models, Dr. Ryozo Noguchi for giving an insight into strain measurement with electronic strain gages and lending his Metex multimeter, Mr. Tsuyoshi Honma for fabricating experimental models and allowing the author to learn their fabrication techniques, and Mr. Akinori Sato for guiding the author to supercomputer and workstation facilities for finite element computation in the Science and Information Processing Center, University of Tsukuba.

Acknowledgement is also due to the Ministry of Education, Japanese

Government for providing a scholarship for the first 4 years of his study here. Without the scholarship, he would not be in Japan to do this research.

Thanks also to the author's friends: Mr. Prathuang Usaborisut, Mr. Weerachai Ajharn, Mr. Lilik Soetiarso, Mr. Tomoyuki Furuichi, and Mr. Hideto Kurosaki for their jokes and joyous company during the writing of the manuscript that kept the author's hope high; Mr. Norihiro Hoshi for very nice cooperation while being together with the author spending cold winter nights in the laboratory and helping the preparation of loading tests, Mr. Takehide Inahata for patiently answering questions when the author fall into problems with Japanese Language especially kanji, and Mr. Eulito Bautista for willingly proofreading some sections of Chapter 2 of this thesis.

Finally, it is to his family. Mere words cannot convey the heartfelt gratitude to the author's wife, Dhinar, who constantly give tireless support, encouragement and understanding during his stay here, especially for the final year of his study in Japan. Also to his sons Ghazy Raksakarama and Eiji Muzaffar, who allowed the author to spend far longer time in the laboratory to study instead of in the dormitory to play with them.

References

1) ASM. 1979. Metal Handbook Vol. 2: Property and selection of nonferrous alloys and pure metals, 9th Ed. American Society of Metals, Metal Park, Ohio.
2) Anonymous. 1992. Metals data book: JIS and main foreign standards, 3rd Ed. The Japanese Standard Association, Tokyo (In Japanese).
3) Ashby, M.F., Jones, D.R.H. 1980. Engineering materials: An introduction to their properties and applications. Pergamon Press, Oxford, England.
4) Atrek, E., Gallagher, R.H., Ragsdell, K.M., Zienkiewicz, O.C. 1984. New directions in optimum structural design. John Wiley and Sons Inc., Chichester, England.
5) Bell, L.H. 1982. Industrial noise control: Fundamentals and applications, 1st Ed. Marcel Dekker Inc., New York.
6) Birch, S. 1994. Aluminum space frame technology. Automotive Engineering, 102(1): 70-73.
7) Birch, S. 1995. Aluminum composite drive shaft. Automotive Engineering, 104(2): 87-90.
8) Bureau of Statistics, US Department of Commerce. 1999. Import of steel products. Washington D.C.
9) Clark, R.L., van de Linde, R. 1993. A rapid automatic tractor ballast system. Transactions of the ASAE, 36(5):1261-1266
10) Clijmans, L., Ramon, H., De Baerdermaeker, J. 1998. Structural modification effects on the dynamic behavior of an agricultural tractor. Transactions of the ASAE, 41(1): 5-10.
11) Clough, R.W., Penzien, J. 1975. Dynamics of structures. McGraw-Hill Book Co. Inc., New York, N.Y.
12) Compton, W.D., Gjostein, N.A. 1990. Materials for ground transportation. Scientific American,112(1): 75-82.
13) Cowell. P.A., Sarfert, A., Austen, J.R. 1994. The lateral stability and dynamic behavior of tractor front linkages. Journal of Agricultural Engineering Research, 58(2): 145-157.
14) Dove, R.C., Adams, P.H. 1984. Experimental stress analysis and motion measurements. Charles E. Merril Books Inc., Columbus, O.H.

15) Dwyer, M.J. 1984. The tractive performance of wheeled vehicles. Journal of Terramechanics, 21(1):19-34.
16) Fenner, D.N.: Engineering stress analysis: A finite element approach. Ellis Horwood Ltd., Chichester, England
17) Garner, D.R. 1967. Analysis of a tractor frame. Farm Machine Design Engineering, 1: 27-32.
18) Gee-Clough, D. 1985. The special problem of wetland traction and flotation. Journal of Agricultural Engineering Research 32(2): 279-288.
19) Gee-Clough, D., Pearson, G., McAllister, M. 1982. Ballasting wheeled tractors to achieve maximum power output in frictional-cohesive soils. Journal of Agricultural Engineering Research, 27(1): 1-19.
20) Gu, Y., Kushwaha, R.L. 1994. Dynamic load distribution and tractive performance of a model tractor. Journal of Terramechanics, 31(1): 21-39.
21) Göhlich, H. 1984. The development of tractors and other agricultural vehicles. Journal of Agricultural Engineering Research, 29(1): 3-16.
22) Håkansson, I., Medvedev, V.W. 1995. Protection of soils from mechanical overloading by establishing limits for stresses caused by heavy vehicles. Soil and Tillage Research, 35: 85-97.
23) Håkansson, I., Reeder, R.C. 1994. Subsoil compaction by vehicle with high axle load: Extent, persistence and crop response. Soil and Tillage Research, 29: 277-304.
24) Hasegawa H., Koike, M., Konaka, T. 1997. Static elastic-plastic analysis for the monocoque-type frame of an agricultural tractor: Numerical simulation using NISA II. Journal of the Japanese Society of Agricultural Machinery, 59(1):11-20 (In Japanese).
25) Hasegawa, H., Koike, M., Konaka, T., Takigawa, T. 1994. Modal analysis of monocoque-type chassis frame of an agricultural tractor. Journal of the Japanese Society of Agricultural Machinery, 56(5): 3-11 (In Japanese).
26) Hossdorf, H. 1980. Model analysis of structures (English Translation by C. van Amerongen). Van Nostran Reinhold Co. Ltd., New York.
27) Hull, D. 1981. An introduction to composite materials. Cambridge University Press, Cambridge, England.
28) Ikemi, T., Li, J., Matsuoka, T., Doi, E. 1997. A study on the front-hitch system of a tractor. Journal of the Japanese Society of Agricultural

Machinery, 59(3): 65-72 (In Japanese).
29) Inooku, K., Nishizaki, K. 1991. Study on durability of a tractor (Part 5): Method of actual loading simulation. Proceedings of the 50th Annual Meeting of the Japanese Society of Agricultural Machinery. JSAM, Tokyo: 59-60 (In Japanese).
30) International Technology Research Institute, World Technology Evaluation Center. 1995. JTECH panel report on advanced materials. Loyola College, Baltimore, M.D.
31) Janeway, R.N. 1975. Human vibration tolerance criteria and application to ride evaluation. SAE Paper No. 75-0166, SAE, Warrendale, P.A.
32) Koike, M., Tanaka, T. 1976. Analysis on the structural strength of tractor frame (Part 2): On the structural damping. Journal of the Japanese Society of Agricultural Machinery, 38(1):19-24 (In Japanese).
33) Koike, M., Tanaka, T. 1977. Analysis on the structural strength of tractor frame (Part 3): On the fatigue strength of rear axle housing. Journal of the Japanese Society of Agricultural Machinery, 38(2):169-175 (In Japanese).
34) Kooistra, M.J., Boersma, O.H. 1994. Subsoil compaction in Dutch marine sandy loams: Loosening practices and effects. Soil and Tillage Research, 11: 1-10.
35) Langhaar, H.L. 1951. Dimensional analysis and theory of models. John Wiley and Sons Inc., New York.
36) Liljedahl, J.B., Turnquist, P.K., Smith, D.W, Hoki, M. 1996. Tractors and their power units, 4th Ed. ASAE, St. Joseph, M.I.
37) Litalien M., Tremblay, F., Rosenfeld, A., Thomas, M., Gesing, A. 1997. Processes for the recycling of sheet and other wrought alloys from aluminum intensive vehicles. SAE Paper No. 97-0126, SAE, Warrendale, P.A.
38) Matthews, J. 1966. Ride comfort for tractor operators IV: Assessment of the ride quality of seats. Journal of Agricultural Engineering Research, 2(1): 44-57.
39) Miki, H. 1988. Development of a new concept tractor. Preprints for the Workshop Regarding the Theme and Prospect for Development of Agricultural Tractor (Volume 2). JSAM, Tokyo: 23-30 (In Japanese).
40) Motobayashi, K. 1992. Basic studies on the optimization of tractor members. Doctoral Dissertation, University of Tsukuba, Tsukuba,

41) Motobayashi, K., Koike, M., Konaka, T. 1993. Optimum design of tractor member by finite element method (Part 2): Shape optimization analysis for a chassis frame. Journal of the Japanese Society of Agricultural Machinery, 55(4): 3-11 (In Japanese).
42) Nagy, I.I. 1973. Finite element method in automobile design. Proc. of the 1973 Tokyo Seminar on Finite Element Analysis. University of Tokyo Press, Tokyo: 444-460.
43) Nishizaki, K., Inooku, K. 1991. Study on durability of a tractor (Part 4): Data acquisition of actual loading and its analysis. Proceedings of the 50th Annual Meeting of the Japanese Society of Agricultural Machinery. JSAM, Tokyo: 17-18 (In Japanese).
44) Office of Technology Assessment. 1991. Improving automobile economy: New standards, new approaches, OTA-E-504. Washington D.C.
45) Oldeman, L.R., Hakkeling, R.T.A., Sombroek, W.G. 1991. World map of the status of human-induced soil degradation: An explanatory note. *In* Soane, B.D., van Ouwerkerk, C. Implications of soil compaction in crop production for the quality of the environment. Soil and Tillage Research, 35: 5-22.
46) Overbagh, W.H. 1995. Aluminum automotive space frames. Automotive Engineering, 103(8): 81-85.
47) Overbagh, W.O. 1995. Use of aluminum in automotive space frames. SAE Paper No. 950721, SAE, Warrendale, P.A.
48) Rahama, O.A., Chancellor, W.J. 1994. Peak and averaged loads on tractor structures. Transactions of the ASAE, 37(6):1733-1740.
49) Raney, J.P., J.B. Liljedahl, R. Cohen. 1961. The dynamic behavior of farm tractors. Transactions of the ASAE, 4(2):215-218.
50) Rhenius, K. Th. 1994. Trends in tractor design with particular reference to Europe. Journal of Agricultural Engineering Research, 57(1): 3-22.
51) Salokhe, V.M., Manzoor, S., Gee-Clough, D. 1990. Pull and lift forces acting on single cage wheel lugs. Journal of Terramechanics 27(1):25-39.
52) Sharp, M.L. 1992. Behavior and design of aluminum structures. McGraw-Hill Book Co. Inc., New York.
53) Singer, F.L. 1962. Strength of materials, 2nd Ed. Harper and Row Publishers Inc., New York.
54) Smith, D.W. 1977 Computer simulation of tractor ride for design evaluation. SAE Paper No. 77-0704, SAE, Warrendale, P.A.

55) Tanaka, T. 1984. Operation in paddy fields: State-of-the-art report. Journal of Terramechanics 21(2):153-179.
56) Taniguchi, T. 1990. Tractor design and development in the next era. Preprints for the International Tractor Symposium. The Hokkaido Branch of the JSAM, Tokachi, Japan: 95-128 (In Japanese).
57) Thompson, W.T. 1981. Theory of vibration with applications, 2nd Ed. Prentice-Hall Inc., Englewood Cliffs, N.J.
58) Timoshenko, S.P., Gere, J.M. 1961. Theory of elastic stability, 2nd Ed. McGraw-Hill Kogakusha Ltd., Tokyo.
59) Timoshenko, S.P., Young, D.H. 1968. Elements of strength of materials, 5th Ed. D. Van Nostrand Co. Inc. and Maruzen Co. Ltd., Tokyo.
60) Timoshenko, S.P., Young, D.H., Weaver, W. 1974. Vibration problems in engineering, 4th Ed. John Wiley and Sons Inc., New York, N.Y., 1974.
61) Tipton, S.M. 1996. Static and fatigue design. *In* Rothbart, H.A. Mechanical Design Handbook. McGraw-Hill Book Co. Inc., New York: 7.3-7.73.
62) Tompstone, R.G., Cowell, P.A. 1990. The influence of front linkage geometry on tractor-implement interaction. Journal of Agricultural Engineering Research, 45(2):175-186.
63) Tsai, S.W., Hahn, H.T. 1980. Introduction to composite materials. Technomic Publishing Co. Inc., Lancaster, Penn.
64) US Geological Survey 1999. Mineral commodity summaries. Washington. D.C.
65) Volterra, E., Gaibes, J.H. 1971. Advanced strength of materials. Prentice-Hall Co. Ltd., Englewood Cliffs, N.J.
66) Zhang, N. Q., Chancellor, W. 1989. Automatic ballast position control for tractors. Transactions of the ASAE, 32(4):1159-1164.
67) Zienkiewicz, O.C. 1977. The finite element method, 3rd Ed. McGraw-Hill Book Co. Inc., Berkshire, England.

Appendix A

Experimental models

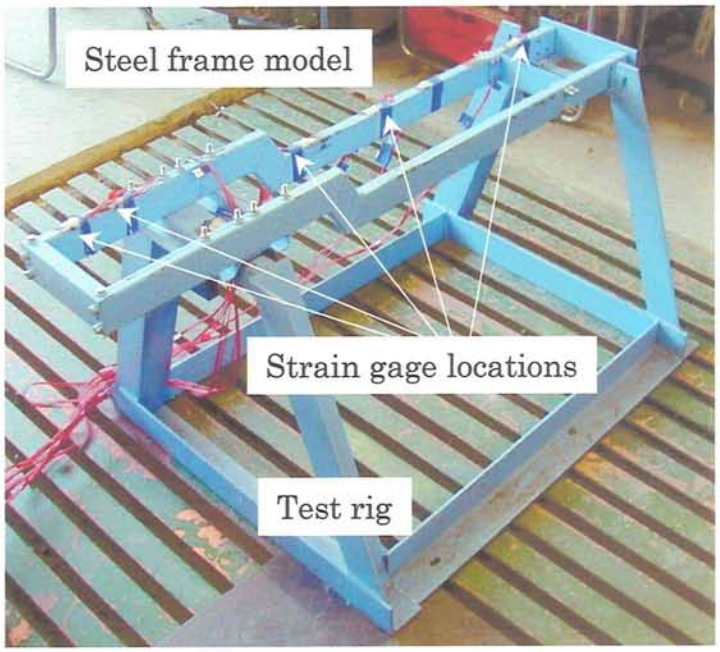

(a) Steel model

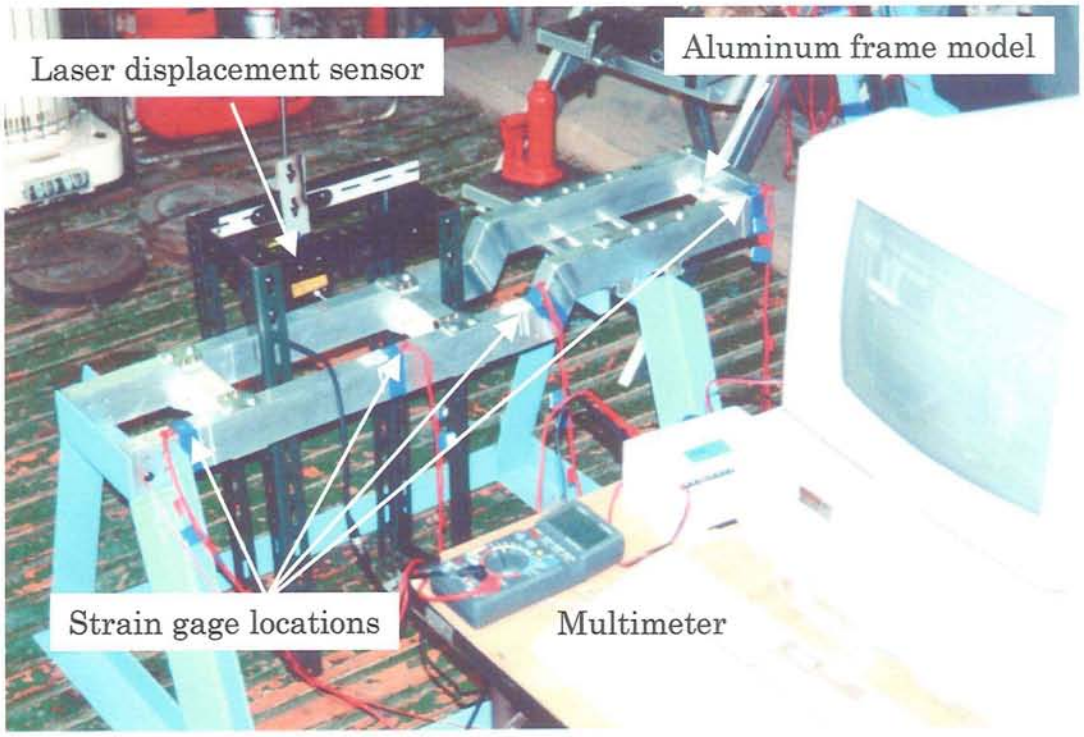

(b) Aluminum model

Appendix B

Selected parts of input data for elastic analysis of aluminum model

```
FEM     IOAREA     25500SAVEBLK      800
$------1-------2-------3-------4-------5-------6-------7-------8-------9-------0
ID
TITLE   Full aluminum model: loading 1-8(alr.i)
SOL             0                                                  : Solution: Static analysis
GRDPNT          0       1                                          : Computing mass property
LIST            1       1       1MAX
PRINT           0       0       0       0       0
SAVE           70
AUTOSPC YES
SUBCASE  1
SUBTITLE CASE  1                                                   : Title for Loading case-1
SPC             1                                                  : Constraint set-1
LOAD            1                                                  : Load set-1
SUBCASE  2
SUBTITLE CASE  2                                                   : Title for Loading case-2
SPC             1                                                  : Constraint set-1
LOAD            2                                                  : Load set-2
SUBCASE  3
```

```
SUBTITLE CASE  3          : Title for Loading case-3
SPC            1          : Constraint set-1
LOAD           3          : Load set-2
SUBCASE  4
SUBTITLE CASE  4          : Title for Loading case-4
SPC            1          : Constraint set-1
LOAD           4          : Load set-4
SUBCASE  5
SUBTITLE CASE  5          : Title for Loading case-5
SPC            1          : Constraint set-1
LOAD           5          : Load set-5
SUBCASE  6
SUBTITLE CASE  6          : Title for Loading case-6
SPC            6          : Constraint set-6
LOAD           6          : Load set-6
SUBCASE  7
SUBTITLE CASE  7          : Title for Loading case-7
SPC            7          : Constraint set-7
LOAD           7          : Load set-7
SUBCASE  8
SUBTITLE CASE  8          : Title for Loading case-8
SPC            8          : Constraint set-8
LOAD           8          : Load set-8
```

```
$------1-------2-------3-------4-------5-------6-------7-------8-------9-------0
BEGIN   BULK
GRID           1                                                                : Geometrical definition of model
GRID           2                       .0300000
GRID           3                       .0600000
  .            .             .       .       .
  .            .             .       .       .
  .            .             .       .       .
GRID         647         .9750000.1935000.0800000
GRID         648         .9750000.1935000.1100000
$------1-------2-------3-------4-------5-------6-------7-------8-------9-------0
SPC1           1  123456       1                                                : Constraints set-1
SPC1           1  123456       6
SPC1           1  123456       4
SPC1           1       3     413
SPC1           1       3     516
SPC1           1       3     488
SPC1           1       3     441
  .            .       .      .
  .            .       .      .
  .            .       .      .
SPC1           1       3     443
$------1-------2-------3-------4-------5-------6-------7-------8-------9-------0
```

```
SPC1           8  123456       3                                          : Constraints set-8
SPC1           8  123456       4
SPC1           8  123456      16
$------1-------2-------3-------4-------5-------6-------7-------8-------9-------0
CQUADE         1       2       4       1      17      20                  : Definition of elements
CQUADE         2       2       1       2      18      17
CQUADE         3       2       2       3      19      18
CQUADE         4       2       5       3      19      21
CQUADE         5       2       6       4      20      22
CQUADE       656       2     648     645     644     647
$------1-------2-------3-------4-------5-------6-------7-------8-------9-------0
PQUADE         1       11.0000001.000000                                  : Property of elements
PQUADE         2       1.0025000.0025000
PQUADE         3       1.0030000.0030000
PQUADE         4       1.0055000.0055000
PTRIAE         5       1.0050000.0050000
$------1-------2-------3-------4-------5-------6-------7-------8-------9-------0
MAT1           1.6830+10.2355+10.45000002700.000                          : Material property
GRAV          10            9.81                    -1.0                  : Self weight due to gravitation
FORCE         11     178          187.5                    -1.0           : Forces in loading set-1
FORCE         11     184          187.5                    -1.0
FORCE         11     331          187.5                    -1.0
FORCE         11     342          187.5                    -1.0
```

```
FORCE          11      516           125.0                    -1.0
FORCE          11      524           125.0                    -1.0
.               .       .             .                        .
.               .       .             .                        .
.               .       .             .                        .
$------1-------2-------3-------4-------5-------6-------7-------8-------9
FORCE          81      116           110.2              1.0                 : Forces in loading set-8
FORCE          81      114           110.2              1.0
FORCE          81       75          3271.7                        1.0
FORCE          81       89          3271.7                       -1.0
$------1-------2-------3-------4-------5-------6-------7-------8-------9
LOAD            1    1.0     1.0       11    1.0       10                  : Load set for case-1
.               .     .       .        .     .         .
.               .     .       .        .     .         .
.               .     .       .        .     .         .
LOAD            8    1.0     1.0       81    1.0       10    1.0       11  : Load set for case-8
ENDDATA
```

Appendix C
Selected parts of output from static analysis on aluminum model

```
* * * * * * * * * * * * * * * * * * * * * *
* * * * * * * * * * * * * * * * * * * * * *
* *                                       * *
* *                                       * *
* *                                       * *
* *              F E M 5                  * *
* *                                       * *
* *      FINITE ELEMENT METHOD 5          * *
* *                                       * *
* *                 25 VERSION            * *
* *                                       * *
* *                 11 LEVEL              * *
* *                                       * *
* *              OCT 01, 1995             * *
* *                                       * *
* *                                       * *
* *                                       * *
* * * * * * * * * * * * * * * * * * * * * * *
* * * * * * * * * * * * * * * * * * * * * * *
```

D I S P L A C E M E N T V E C T O R

POINT ID.	TYPE	CD ID.	T1	T2	T3	R1	R2	R3
1	G		0.000000d+00	0.000000d+00	0.000000d+00	0.000000d+00	0.000000d+00	0.000000d+00
2	G		0.000000d+00	0.000000d+00	0.000000d+00	0.000000d+00	0.000000d+00	0.000000d+00
3	G		4.287165d-06	-5.020283d-07	-9.333627d-08	3.243963d-05	0.000000d+00	5.870308d-06

Node number	*x-direction*	*y-direction*	*z-direction*	θ_x*-direction*	θ_y*-direction*	θ_z*-direction*

F O R C E S O F S I N G L E - P O I N T C O N S T R A I N T

POINT ID.	TYPE	CD ID.	T1	T2	T3	R1	R2	R3
231	G		0.000000d+00	0.000000d+00	0.000000d+00	1.068590d-15	0.000000d+00	0.000000d+00
238	G		0.000000d+00	0.000000d+00	0.000000d+00	-1.172673d-15	0.000000d+00	0.000000d+00
250	G		0.000000d+00	0.000000d+00	0.000000d+00	-1.231092d-09	0.000000d+00	0.000000d+00
256	G		0.000000d+00	0.000000d+00	0.000000d+00	1.231032d-09	0.000000d+00	0.000000d+00
277	G		0.000000d+00	0.000000d+00	0.000000d+00	4.440892d-16	0.000000d+00	0.000000d+00

SUBCASE 1

F O R C E S A N D S T R E S S E S I N Q U A D R I L A T E R A L E L E M E N T S (Q U A D E)

ELEMENT ID.	FIBER DISTANCE	FORCE.... STRESS...	MX NORMAL-X	MY NORMAL-Y	MXY SHEAR-XY	ANGLE	MAJOR	MINOR	MAX-SHEAR
1			3.437307d-01	9.089170d-02	-3.015154d-02				
	-8.000000d-04		-4.289562d+05	-2.033353d+05	9.019011d+04	70.6791	-1.717143d+05	-4.605772d+05	1.444315d+05
	8.000000d-04		1.182282d+06	2.227195d+05	-5.114526d+04	-3.0424	1.185000d+06	2.200011d+05	4.824994d+05
2			3.926944d-02	1.116350d-02	-1.535712d-02				
	-8.000000d-04		-4.387561d+05	7.025373d+04	-3.347195d+05	-63.6238	2.362365d+05	-6.047389d+05	4.204877d+05

F O R C E S A N D S T R E S S E S I N T R I A N G U L A R E L E M E N T S (T R I A E)

ELEMENT ID.	FIBER DISTANCE	FORCE.... STRESS...	MX NORMAL-X	MY NORMAL-Y	MXY SHEAR-XY	ANGLE	MAJOR	MINOR	MAX-SHEAR
278			-5.617234d+00	-2.177598d+00	2.264438d-01				
	-8.000000d-04		6.496859d+06	6.383790d+06	8.801408d+06	44.8160	1.524191d+07	-2.361265d+06	8.801589d+06
	8.000000d-04		-1.983393d+07	-3.823702d+06	9.862863d+06	64.5321	8.738583d+05	-2.453149d+07	1.270267d+07

**** END OF ANALYSIS. MODEL ID = , ANALYSIS STATUS 0 ****

Appendix D
Results of verification of eigenvalue analysis module

1. Cantilever plate, shell element

Mode	Theory[70]	FEM5	Error,%
1	3.01	2.92	2.99
2	7.37	7.58	2.84
3	18.50	19.04	2.91
4	23.65	25.73	8.79
5	26.89	28.13	4.60

2. Simply supported square plate

Mode	Theory[70]	FEM5	Error,%
1	84.10	84.56	0.55
2	210.24	214.32	1.94
3	210.24	214.32	1.94
4	336.38	343.26	2.04
5	420.47	435.25	3.52

3. Free edged square plate, shell element

Mode	Theory[70]	FEM5	Error,%
1	55.18	56.02	1.52
2	80.46	82.26	2.23
3	93.58	98.53	5.30

4. Cantilever beam, bar

Mode	Theory[18]	FEM5	Error,%
1	10.25	10.30	0.54
2	64.22	65.01	1.24
3	179.83	180.21	0.21

5. Simply supported beam, bar

Mode	Theory[18)]	FEM5	Error,%
1	28.77	28.77	0.01
2	115.06	114.13	0.81
3	258.89	261.33	0.94

6. Unconstrained beam, bar

Mode	Theory[67)]	FEM5	Error,%
1	65.29	66.12	1.28
2	179.83	182.32	1.38
3	352.66	360.32	2.17

7. Cantilever beam using solid element

Mode	Theory[70)]	FEM5	Error,%
1	0.56	0.56	0.089
2	3.51	3.6	2.660
3	9.82	10.1	2.851
4	19.24	19.52	1.436
5	31.81	33.02	3.808
6	31.81	33.02	3.808
7	66.37	70.06	5.566